**Table 1 – Distribution of GlcAT transcripts in adult mouse brain**

| | GlcAT-P | GlcAT-S |
|---|---|---|
| *Olfactory system* | | |
| Olfactory bulb | | |
| Glomerular layer | ++ | ++ |
| Mitral cell layer | ++ | 0 |
| Anterior olfactory nu. | +++ | 0 |
| *Basal forebrain* | | |
| Caudate putamen/globus pallidus | +/++[a] | 0 |
| Ventral pallidum | ++[a] | + |
| Stria terminalis | + | + |
| Substantia nigra pars compacta | +++[a] | 0 |
| Lateral septum | +++ | ++ |
| Medial septum/diagonal band | ++ | + |
| *Amygdaloid complex* | | |
| Central/medial amygdaloid nu. | ++ | + |
| Amygdalohippocampal area | + | ++ |
| *Hippocampal formation* | | |
| Hippocampus | | |
| CA1 subfield | +++ | ± |
| CA2/CA3 subfield | +++ | +++ |
| Dentate granule cell layer | +++ | 0 |
| Dentate polymorphic layer | ++++[a] | 0 |
| *S. oriens*/lucidum/radiatum | ++[b] | ++[b] |
| *S. lacunosum*-moleculare | 0 | 0 |
| Subiculum | + | ++ |
| *Cerebral cortex* | | |
| Isocortex layers | | |
| I | 0 | 0 |
| II | +++ | 0 |
| III | ± | 0 |
| IV | ++ | ++[d] |
| V | +++ | +++[a] |
| VI | +++ | +++[a] |
| Orbital cortex | ++ | ++[a] |
| Piriform cortex | +++ | + |
| Indusium griseum | ± | ++ |
| Ectorhinal cortex | +++ | +++ |
| Endopiriform cortex | +[c]/++ | +++ |
| Claustrum | ++ | +++ |
| Cingulate/retrosplenial cortices | ++ | ++[b] |
| *Thalamus* | | |
| Ventroposterior/posterior nu. | + | + |
| Lateral/medial geniculate nu. | + | ++/+++ |
| Ventrolateral/ventromedial | ++ | 0 |
| Anteroventral/anterodorsal thalamic nu. | ++/++ | ++/+++ |
| Anteromedial/mediodorsal nu. | ++ | ++ |
| Paraventricular/centromedial nu. | +++/+ | +++/++ |
| Paracentral/centrolateral nu. | + | + |
| Rhomboid/reuniens nu. | ++ | + |
| Parafascicular nu. | + | ++ |
| Reticular nu. | + | ± |
| Medial/lateral habenular nu. | ++++/+++[a] | 0/++ |
| *Hypothalamus* | | |
| Dorsomedia hypothalamic nu. | + | ++ |
| Ventromedial hypothalamic nu. | +++ | ++ |
| Arcuate hypothalamic nu. | 0 | +++ |
| Lateral hypothalamic nu. | + | + |
| Supraammillary nu. | ++ | ++ |
| *Hypothalamus* | | |
| Medial/lateral mammilary nu. | + | 0 |
| Pretectal nu. group | + | + |
| *Midbrain and pons* | | |
| Superior/inferior colliculus | ++/+++ | +/++[a] |
| Periaquidauctal gray | + | + |
| Interpeduncular nu. | +++ | ++[a] |
| Red nu. | ± | ++[a] |
| Lateral lemuniscus | +++ | ++ |
| Pontine/reticulotegmental nu. | ++ | ±/++ |
| Pontine reticular field | + | ± |
| Dorsal tegmental nu. | +++ | ++ |
| Parabrachial nu. | +++ | ++ |
| Parabigeminal nu. | ++++ | ++ |
| Dorsal/median raphe nu. | ++ | + |
| Superior olive | ++ | 0 |
| *Medulla* | | |
| Giantcellular reticular nu. | ++[a] | ± |
| Raphe magnus/pallidus/obscurus nu. | + | + |
| Inferior olive/lateral reticular nu. | 0 | 0 |
| Cuneate nu. | ++ | + |
| *Cranial nerve nuclei* | | |
| Oculomotor (3) | +++ | ++ |
| Trigeminal nu. (5) | | |
| Motor trigeminal nu. | + | ± |
| Ventrolateral trigeminal nu. | +++ | ++ |
| Spino-trigeminal nu. | +++ | + |
| Principal sensory trigeminal nu. | +++ | + |
| Mesencephalic trigeminal nu. | +++[b] | 0 |
| Vestibular nu. group(8) | ++ | ++ |
| Cochlear nu. group | +++ | ++ |
| Prepositus hypoglossal nu. | + | ++ |
| *Cerebellum* | | |
| Molecular cell layer | + | ± |
| Purkinje cell layer | +++ | ± |
| Granular cell layer | 0 | + |
| Deep cerebellar nu. | +++ | ± |
| *Others* | | |
| Choroid plexus | 0 | 0 |
| Ependyma and pia mater | 0 | 0 |
| Subfornical organ | 0 | ++ |

nu., nucleus; ++++, very high; +++, high; ++, moderate; +, low; ±, very low; 0, less than threshold.
[a]A few cells positive for mRNA.
[b]Few cells positive for mRNA.
[c]In the anterior part.
[d]In the parietal cortex, there were few cells positive for mRNA.
In GlcAT-P-deficient mouse brains, there were no signals using GlcAT-P cRNA. There were no differences in the distributions of GlcAT-S mRNA in brains between wild-type and GlcAT-P-deficient mice.

containing cells expressed with GlcAT-S mRNA between wild-type and GlcAT-P-deficient mice (data not shown).

Next we performed immunohistochemistry to investigate the distribution of HNK-1 carbohydrate epitope, which is synthesized by GlcAT enzymes (Fig. 2 and Table 2) and

compared the regions expressing the GlcAT enzymes with the areas containing HNK-1 carbohydrate in the adult mouse brain with or without the GlcAT-P gene. First, in the wild-type mice, the HNK-1 carbohydrate was widely distributed over most of the mouse brain, which reflected the expression patterns of the GlcAT-P mRNAs. Especially, among regions containing a high level of GlcAT-P mRNA, the lateral septum (LS; Figs. 2B-a and j), the hippocampal complex (Hip; Figs. 2A-c and h), and the interpeduncular nucleus (IP; Figs. 2A-d and i) in the limbic system and the cochlear nucleus (VC; Figs. 2A-e and j) and the lateral lemuniscus (LL; Figs. 2B-b, h, k, and q), the inferior colliculus (IC; Figs. 2A-e and j), the parabigeminal nucleus (PBG; Figs. 2B-b, e, k, and n), the parabrachial nuclei (PB; Figs. 2A-e and j), and the trigeminal sensory system (Pr5; Figs. 2A-e and j), and the dorsal column nuclei (Cu; Figs. 2B-d and m) in the sensory system showed very intense staining of the HNK-1 antibody. On the other hand, among areas containing little GlcAT-P or GlcAT-S mRNAs, the medial nuclei of the bed nucleus of the stria terminalis (BST; Figs. 2A-b and g), the reticular nucleus of the thalamus (Rt; Figs. 2A-c and h), and the precerebellar nuclei containing the inferior olive (IO; Figs. 2B-f and o), and the lateral reticular nucleus (LRt; Figs. 2B-i, o, and r), expressed the HNK-1 carbohydrate diffusely. These nuclei also expressed the HNK-1 carbohydrate strongly in GlcAT-P-deficient mouse brain. In addition, the SFO, the Arc, and the MG, which showed very intense signals of GlcAT-S mRNA, contained little HNK-1 carbohydrate in mice with or without GlcAT gene.

In the present study, we also compared the HNK-1 carbohydrate expression in the layer of the cortex and the cerebellum between wild-type and GlcAT-P-deficient mice (Fig. 3). In the cortex, wild-type mice expressed GlcAT-P in layer II to VI (Fig. 3A), which was likely to have led to the expression of HNK-1 carbohydrate in most layers, including very intense signals in the layer II (Fig. 3B). On the other hand, GlcAT-P-deficient mice expressed a little GlcAT-S and HNK-1 carbohydrate in layers V–VI of most of the isocortex (Figs. 1B and 2A-g, h, and i), while in the parietal cortices (Waite, 2004), the presence of GlcAT-S was observed in layers V–VI (Fig. 3C) and the presence of HNK-1 carbohydrate in layers III to VI (Fig. 3D). In the cerebellum of wild-type, the purkinje cells expressed GlcAT-P (P; Fig. 3E) and the molecular layer strongly contained high levels of HNK-1 carbohydrate (M; Fig. 3F). In addition, HNK-1 signals were also seen as several neuronal spots in the granular cell layers of the wild-type and GlcAT-P-deficient mice (arrowhead in G; Fig. 3F) and the dotted signals still left in the granular layer of GlcAT-P-deficient mice (arrowheads in G; Fig. 3H), which seemed to be due to the presence of GlcAT-S transcripts (white arrowhead in G; Fig. 3G).

### 2.2. *Regulated expression of GlcAT-S in the hippocampus in mice with GlcAT-P deficiency*

We have previously reported that GlcAT-P-deficient mice exhibited reduced long-term potentiation (LTP) at the Schaffer collateral-CA1 synapses (Yamamoto et al., 2002). One matter for concern is whether GlcAT-S compensated for the lack of GlcAT-P enzyme activity for production of HNK-1 in the hippocampus of the GlcAT-P-deficient mice. In the present study, we found that the level of GlcAT-S transcripts in the CA3-subfield of GlcAT-P-deficient mice was higher than that in wild-type, especially an increase of 1.7-fold was observed in the CA3a containing the Schaffer collateral fibers projecting to the CA1-subfield (Figs. 4C, D, and J). The HNK-1 carbohydrate was expressed strongly in the polymorphic layer (Figs. 2A-h and 5H) and the CA3a (Fig. 5E). However, in the strata oriens and radiatum and the pyramidal cell layer of the CA1-subfield, HNK-1 signals were localized mostly in neuronal cells containing parvalbumin signals (Figs. 5A, D, and G), a marker for the interneuron (Kosaka et al., 1987). On the other hand, there were little differences of immunoreactions of HNK-1 or WFA between wild-type and GlcAT-P-deficient mice (Fig. 6).

## 3. Discussion

HNK-1 carbohydrate epitope is a sulfated trisaccharide, $HSO_3$3GlcAβ1-3Galβ1-4GlcNAc (Chou et al., 1986; Voshol et al., 1996), and key enzymes in the biosynthesis of the epitope are two different glucuronyltransferases (GlcAT-P and GlcAT-S) (Seiki et al., 1999; Shimoda et al., 1999; Terayama et al., 1997, 1998). Although these enzymes have different acceptor specificities in vitro assay system (Kakuda et al., 2005), the critical acceptor specificity is dependent on in which cells the enzyme meets with acceptor substrates. In the brain, with its great variations in the cell populations and their connections, it is important to provide information about the expression of these enzymes in the particular cells and fibers. In the present study, we determined directly brain regions containing cells expressing two enzymes by detecting their transcripts not showing displacements and projections. The major findings of the present study were the regional specificities of GlcAT transcripts and HNK-1 carbohydrate epitope.

HNK-1 carbohydrate epitope was distributed widely in the adult mouse brain and there were two patterns of HNK-1 immunostaining: spotted and diffuse signals (Table 2, S and D). Diffuse signals are likely to be brought through efferents from the regions expressing GlcAT transcripts. The epitope was especially concentrated as strong signals in the limbic-related, the sensory, and the cerebellar systems. The present findings suggested that HNK-1 carbohydrate networks tended to be especially concentrated in the septal regions among the limbic-related systems (Risold, 2004). First, GlcAT transcripts and HNK-1 carbohydrate were localized strongly in the lateral septal region (LS), the hippocampus, and the paraventricular thalamic nucleus (PV). These regions are connected as follows: (1) the LS receives ipsilateral afferents from the CA1-subfield and bilateral ones from the CA3-subfield of the hippocampus, (2) axons from the LS innervate the midline nuclei of the thalamus, especially the PV, and (3) afferents from the PV project to the hippocampal formation. Next, the present study also showed that the bed nucleus of the stria terminallis (BST) expressed the HNK-1 carbohydrate very strongly and diffusely, but not GlcAT transcripts. The expression of HNK-1 carbohydrate is reasonable because the stria terminalis is one of four main routes of afferents and efferents of the septal region; the stria terminalis, the fornix,

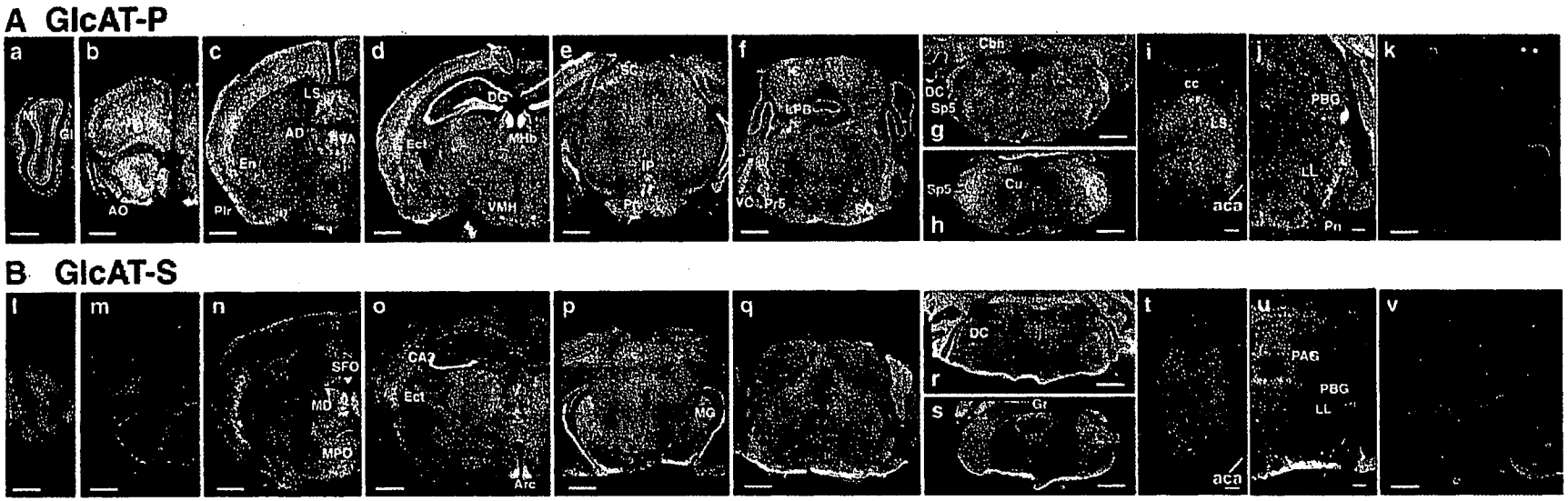


Fig. 1 – Micro-autoradiogram showing GlcAT-P (A) and GlcAT-S (B) cRNA labeling patterns in coronal sections (14 μm thick) of mouse brain. Dark-field images of emulsion-dipped coronal sections in the olfactory structure (a, l); in coronal planes at the level of the olfactory nu. (b, m); at the anterior thalamic nu. (c, n); at the habenular nu. (d, o); at the interpeduncular nu. (e, p); at the inferior colliculus (f, q); at the vestibular nu. (g, r); at the spinal trigeminal nu. (h, s); at the lateral septal nu. (i, t); at the lateral lemuniscus (j, u); at the habenular nu. with sense probe (k, v). Stars indicate artifacts (b, d–f, and o). Scale bar=1 mm in a–h, k, l–s, and v; 400 μm in i, j, t, and u.

the medial forebrain bundle, and the stria medullaris. In addition, the LS connects extensively with the medial zone of the hypothalamus and then the medial zone connects with the medial nuclei of the BST. As the ventromedial hypothalamic nucleus (VMH) in the medial zone of the hypothalamus (Simerly, 2004) expressed both GlcAT mRNAs

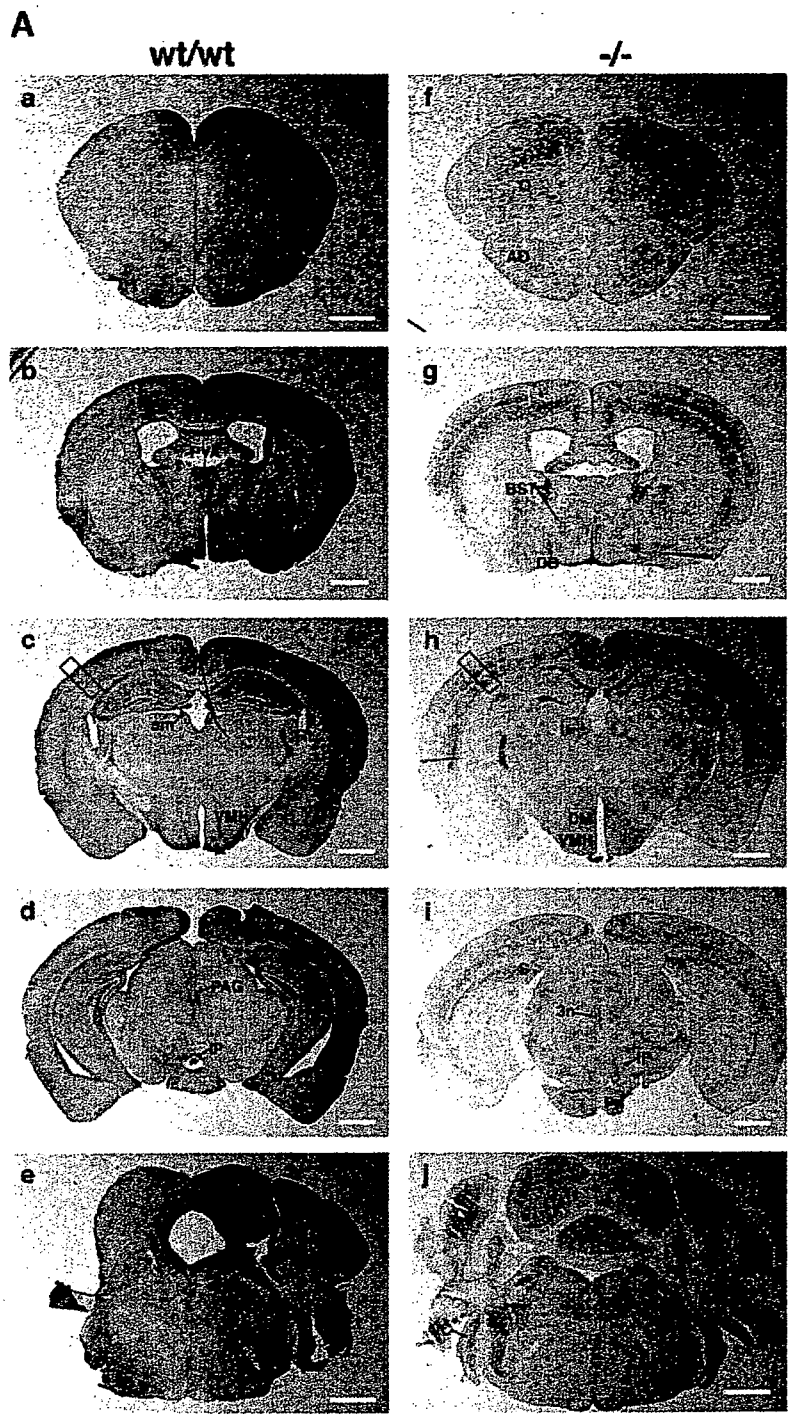


Fig. 2 – Comparison of HNK-1 carbohydrate expressions in the coronal section of GlcAT-P-deficient mice and normal littermates. Representative immunohistochemical micrograph with anti-HNK-1 antibody. Brightfield images of coronal sections (14 μm thick) of mouse brain with (w/w; A-a–e and B-a–i) or without (–/–; A-f–j and B-j–r) GlcAT-P gene. Regions in the rectangles in A-c and A-h are expanded in Figs. 3B and D. Regions in the rectangles in a and j are magnified in the insets (B). Differential interference contrast images (insets of a and j, e, g–i, n, and p–r) (B). Scale bar=1 mm in A; 200 μm as black bars in B; 50 μm as white bars in B.

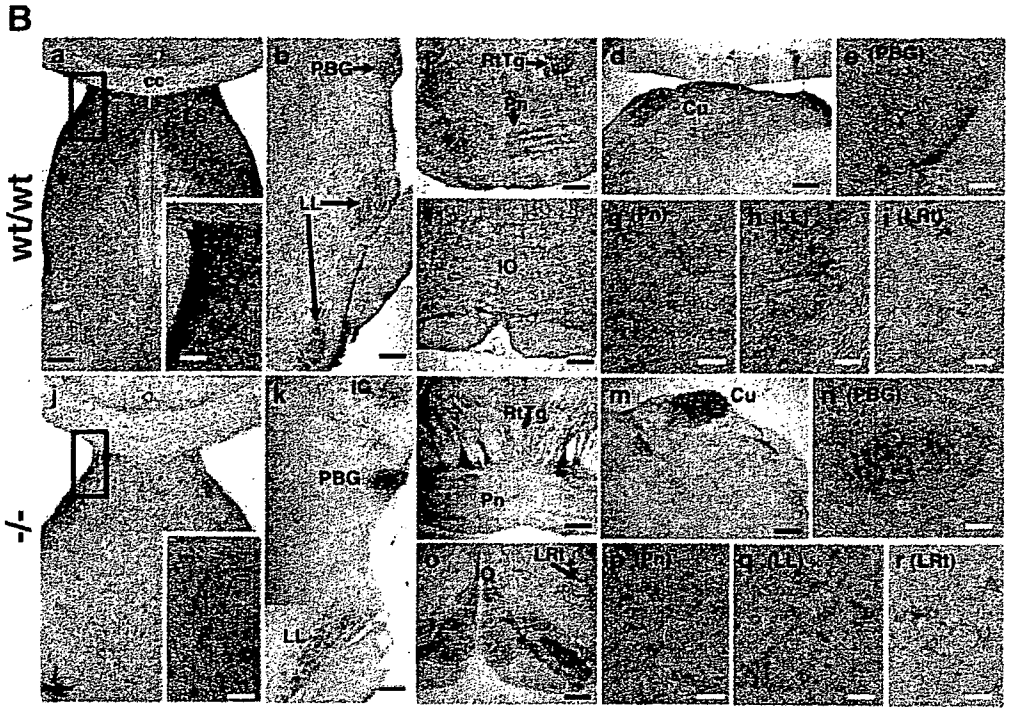


**Fig. 2 (*continued*)**

strongly, the HNK-1 carbohydrate seems to be present at high levels in the BST of both wild-type and GlcAT-P-deficient mice. The LS is also directly connected with the periventricular zone of the hypothalamus. The arcuate hypothalamic nucleus (Arc) in the periventricular zone (Simerly, 2004) expressed GlcAT-S mRNA strongly, which might be involved in any controls of neuroendocrine and aútonomic responses. Finally, there was a system in which the stria medullaris (sm; Fig. 2A-c) and the fasciculus retroflexus (fr; Fig. 2A-h) projected from the septal regions. In this network, the septal afferents project through the stria medullaris to the medial habenular nucleus (MHb) and the projections continue in the fasciculus retroflexus to reach the IP. In this network, very intense expressions of GlcAT-P in the MHb and the IP (Figs. 1A-d and e) seemed to induce very strong expression of HNK-1 carbohydrate in the stria medullaris (sm; Fig. 2A-c) and the IP (Fig. 2A-d). On the other hand, the other neurons in the basal forebrain except for the septum connect with the lateral habenular nucleus (LHb) through the stria medullaris. Therefore, moderate expression of GlcAT-S in the LHb might induce moderate expression of HNK-1 carbohydrate in the fasciculus retroflexus (fr; Fig. 2A-h) and the IP (Fig. 2A-i), as suggested by the results of immunohistochemistry in GlcAT-P-deficient mouse brain. The present study showed that two nuclei showing expression of GlcAT-P mRNA at the ++++ level (Table 1) were the MHb and the parabigeminal nucleus (PBG). It is reported that these nuclei contain a dense aggregate of cholinergic neurons, while the sept-hippocampal cholinergic pathway contains basal forebrain cholinergic neurons (Butcher, 1995, 2004). It is possible that at least a part of the subpopulations composed of neurons expressing GlcAT-P and then catalyzing the HNK-1 carbohydrate synthesis belong to the cholinergic system.

Kosaka et al. have previously showed that a part of neurons with HNK-1 immunostaining contained $Ca^{2+}$-binding protein parvalbumin (Kosaka et al., 1990, 1992). On the other hand, the present study showed that most neurons with HNK-1 immunostaining were a subpopulation of interneurons immunopositive for parvalbumin in the hippocampus and the cerebral cortices (Fig. 5J) of GlcAT-P-deficient mice. The strong staining of HNK-1 in the hippocampus was induced by the expression of GlcAT-S mRNA in the CA3a. It has been previously reported that LTP was increased by application of anti-HNK-1 antibody into the stratum radiatum (Saghatelyan et al., 2000). The findings of the present study suggest that the antibody was targeted to interneurons expressing the HNK-1 carbohydrate that GlcAT-S synthesized, resulting in the reduction of the efficacy of evoked GABA release. Alternatively, as GlcAT-P was expressed in pyramidal neurons of the CA1–3 subfields, the present study also confirmed a previous report showing that the HNK-1 carbohydrate synthesized by GlcAT-P activity directly affects the increase of LTP at the Schaffer collateral-CA1 synapses (Yamamoto et al., 2002).

Among the sensory systems (Malmierca and Merchán, 2004), the auditory system was most markedly enriched in GlcAT transcripts. For example, the cochlear nuclear complex provides the first relay center in the ascending pathway of the auditory process and the axons project into the lateral lemniscus (LL); especially, afferent projections to the ventral complex of the LL arise mainly from the contralateral side of

**Table 2 – Distribution of HNK-1 in GlcAT-P-deficient mice**

| Olfactory system | +/+ | −/− |
|---|---|---|
| Olfactory bulb | D | N |
| Granular cell layer | | |
| Mitral cell layer | D | N |
| Anterior olfactory nu. | DS | S |
| *Basal forebrain* | | |
| Caudate putamen/globus pallidus | $D^W$ | N/D |
| Ventral pallidum | D | D |
| Stria terminalis | $D^S$ | $D^S$ |
| Substantia nigra pars compacta | N | N |
| Lateral septum | $D^S$ | $S^a$ |
| Medial septum/diagonal band | $D^W$ | $S^a/DS^a$ |
| *Amygdaloid complex* | | |
| Central/medial amygdaloid nu. | D | N |
| Amygdalohippocampal area | D | N |
| *Hippocampal formation* | | |
| Hippocampus[b] | | |
| CA1 subfield | D | S |
| CA2/CA3 subfield | D | S |
| Dentate granule cell layer | D | $S^a$ |
| Dentate polymorphic layer | | |
| *S. oriens*/lucidum/radiatum | $D^S$ | S |
| *S. lacunosum*-moleculare | N | N |
| Subiculum | DS | S |
| *Cerebral cortex* | | |
| Isocortex layers | | |
| I | N | N |
| II | D | N |
| III | D | $S^{ac}$ |
| IV | N | $S^c$ |
| V | DS | S |
| VI | DS | S |
| Orbital cortex | D | S |
| Piriform cortex | $D^W$ | N |
| Indusium griseum | D | $S^a$ |
| Ectorhinal cortex | D | D |
| Endopiriform cortex | D | D |
| Claustrum | D | D |
| Cingulate/retrosplenial cortices | DS | $D^S$ |
| *Thalamus* | | |
| Ventroposterior/Posterior nu. | $D^W$ | $D^W/N$ |
| Lateral/medial geniculate nu. | $D^W$ | N |
| Ventrolateral/ventromedial | $D^W$ | N |
| Anteroventral/anterodorsal thalamic nu. | $D^W$ | $D^W$ |
| Anteromedial/Mediodorsal nu. | $D^W$ | $D^W$ |
| Paraventricular/ centromedial nu. nu. | $D^S/D^W$ | $D^W$ |
| Paracentral/centrolateral nu. | $D^W$ | $D^W$ |
| Rhomboid/reuniens nu. | $D^W$ | $D^W$ |
| Parafascicular nu. | $D^W$ | N |
| Reticular nu. | $D^S$ | $D^S$ |
| Medial/lateral habenular nu. | $D/D^W$ | N/D |
| *Hypothalamus* | | |
| Dorsomedial hypothalamic nu. | D | $D^S$ |
| Ventromedial hypothalamic nu. | $D^S$ | $D^S$ |
| Arcuate hypothalamic nu. | $D^W$ | $D^W$ |
| Lateral hypothalamic nu. | $D^W$ | N |
| Supramammillary nu. | D | $D^W$ |
| Medial/lateral mammilary nu. | D | D |
| Pretectal nu. group | $D^W$ | S |

**Table 2 (*continued*)**

| Olfactory system | +/+ | −/− |
|---|---|---|
| *Midbrain and pons* | | |
| Superior/inferior colliculus | $D^W/D^SS^S$ | $S/S^S$ |
| Periaquiductal gray | $D^S$ | D |
| Interpeduncular nu. | $D^S$ | D |
| Red nu. | $S^a$ | DS |
| Lateral lemuniscus | $S^S$ | $S^S$ |
| Pontine/reticulotegmental nu. | $S/S^S$ | $D/D^S$ |
| Pontine reticular field | $D^W$ | $D^W$ |
| Dorsal tegmental nu. | DS | DS |
| Parabrachial nu. | $D^SS^S$ | $S^S$ |
| Parabigeminal nu. | $D^SS^S$ | $D^SS^S$ |
| Dorsal/median raphe nu. | D | D/S |
| Superior olive | DS | 0 |
| *Medulla* | | |
| Giantcellular reticular nu. | D | $D^w$ |
| Raphe magnus/pallidus/obscurus nu. | D | $D^W$ |
| Inferior olive | D | $DS^{Sd}$ |
| Lateral reticular nu. | D | $D^S$ |
| Cuneate nu. | $D^S$ | $D^S$ |
| *Cranial nerve nuclei* | | |
| Oculomotor (3) | N | $S^S$ |
| Trigeminal nu. | $D^W$ | N |
| Motor trigeminal nu. | DS | $S^S$ |
| Ventrolateral trigeminal nu. | DS | $S^S$ |
| Spino-trigeminal nu. | $D^SS^S$ | $S^S$ |
| Principal sensory trigeminal nu. | $D^SS^S$ | $S^S$ |
| Mesencephalic trigeminal nu. | N | N |
| Vestibular nu. group (8) | D | $S^S$ |
| Cochlear nu. group | $DS^S$ | $S^S$ |
| Prepositus hypoglossal nu. | D | D |
| *Cerebellum* | | |
| Molecular cell layer | D | N |
| Purkinje cell layer | S | N |
| Granular cell layer | $S^a$ | $D^WS^a$ |
| Deep cerebellar nu. | $DS^S$ | $DS^S$ |
| *Others* | | |
| Choroid plexus | N | N |
| Ependyma and pia mater | N | N |
| Subfornical organ | N | N |

nu., nucleus; D, diffuse signals positive for HNK-1; S, spotted signals in cells positive for HNK-1; N, negative.
[a] A few cells were positive for HNK-1.
[b] There were no signals in the hippocampal pyramidal cells of either type of mouse brain.
[c] The spotted signals in layer III and IV were observed only in the parietal cortex.
[d] There was an especially strong signal in the beta subnucleus of the inferior olive.
[W] Weak signals.
[S] Strong signals.

the ventral cochlear nucleus (VC). Then the LL and cochlear nuclei project axons to the inferior colliculus (IC) directly. GlcAT transcripts and HNK-1 carbohydrate were concentrated in these three nuclei. On the other hand, the medial geniculate of the thalamus (MG) contained only GlcAT-S mRNA, but little GlcAT-P mRNA or HNK-1 carbohydrate. The MG, which is the last center for auditory processing before inputs reach the

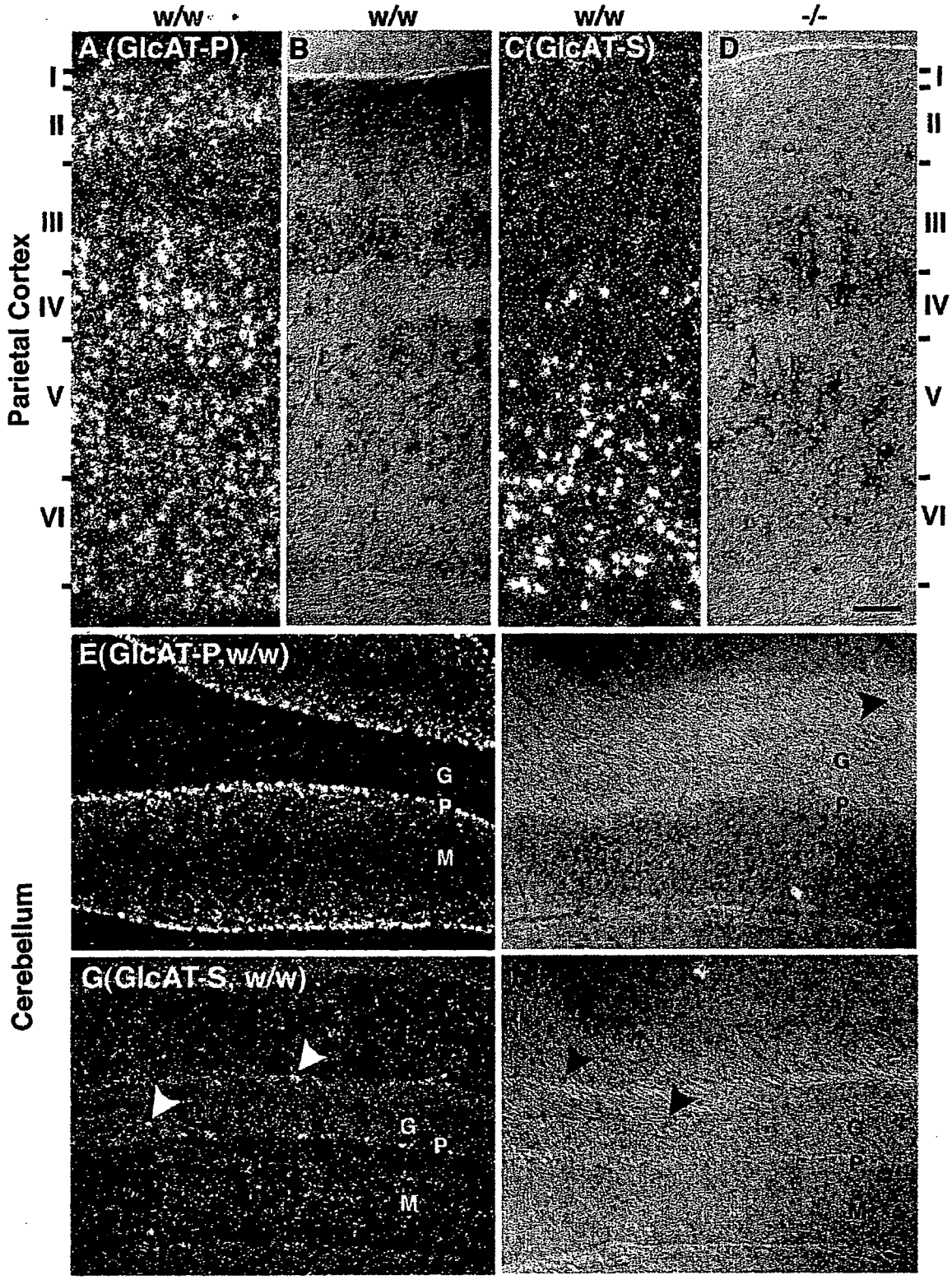


Fig. 3 – Expression of GlcAT transcripts and HNK-1 carbohydrate in the parietal cortex (A–D) and the cerebellum (E–H) of mouse brain. Dark-field images of *in situ* hybridization (A, C, E, and G), differential interference contrast images of immunohistochemistry (B, D, F, and H). I–VI, layers of the cerebral cortex; G, granular cell layer; M, molecular layer; P, Purkinje cell layer of the cerebellum. GlcAT-P (A and E); GlcAT-S (C and G); HNK-1 (B, D, F, and H). Wild-type (A–D, E, F, and G); –/– (D and H). Cellular patterns of GlcAT-S transcript in C and G were the same as those in –/– mice. Scale bar = 100 μm.

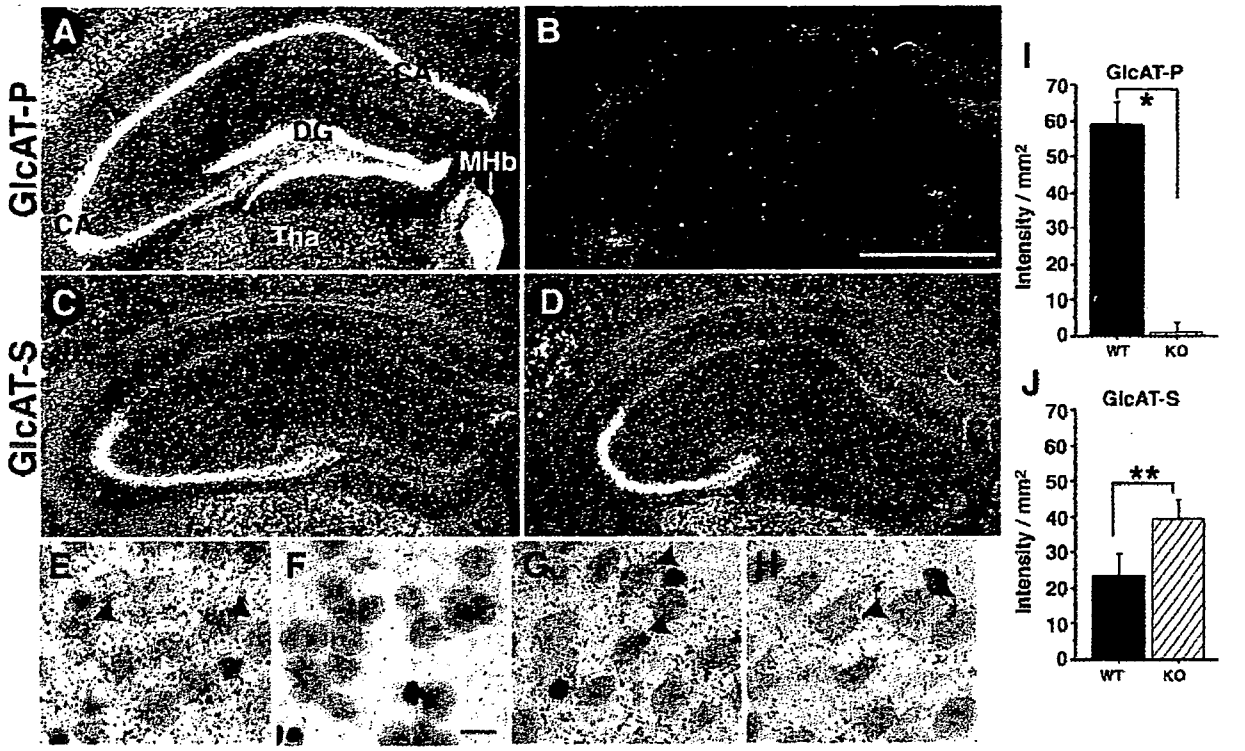


**Fig. 4 – Comparisons of GlcAT transcripts in the hippocampus between wild-type (wt/wt; A, C, E, and G) and GlcAT-P-deficient (−/−; B, D, F, and H) mice. Microautoradiography of *in situ* hybridization in the hippocampus under dark-field illumination (A–D) and bright-field illumination (E–H). Scale bars=1 mm (A–D) and 10 μm (E–H). GlcAT-P cRNA (A, B, E, and F) and GlcAT-S cRNA (C, D, G, and H). Arrowheads show neuronal cells containing signals. Comparisons of GlcAT-P and GlcAT-S transcripts between wild-type and GlcAT-P-deficient mice (I and J). ■ WT, □ GlcAT-P column and vertical line, mean (+SD) signal intensity per mm². Statistical significance of the differences was determined by paired *t*-test (*$p<0.0001$ for GlcAT-P; **$p=0.0014$ for GlcAT-S). The data show the lack of signal of GlcAT-P cRNA in the hippocampus of GlcAT-P-deficient mice (B, F, and I).**

auditory cortex, receives axons from the IC and part of the efferents from the MG project to the reticular nucleus of the thalamus (Rt) containing all GABAergic and parvalbumin-positive neurons. As the Rt showed very strong labeling of HNK-1, several efferents from the MG might contribute to the very strong labeling of HNK-1 in the Rt (Groenewegen and Witter, 2004). On the other hand, the strong labeling in the Rt might also be dependent on projections from layer VI of the cerebral cortex, because afferents to the Rt mainly originate in layer VI. However, like the MG, the Arc and the subfornical organ (SFO) also showed strong positivity of GlcAT-S mRNA but not GlcAT-P mRNA nor HNK-1 carbohydrate. The possibility still exists that GlcAT-S enzyme exerts activity toward another acceptor substrate other than HNK-1 in those nuclei. Concerning the somatosensory system (Tracey, 2004), the cuneate nucleus (Cu) and the gracile nucleus (Gr) expressed GlcAT mRNAs moderately and the HNK-1 carbohydrate very intensely. These nuclei belong to the dorsal column nuclei, which receive somatosensory afferents originated in cell bodies in the dorsal root ganglia. As the dorsal column nuclei also receive afferent fibers from the trigeminal nerve, the trigeminal nuclei expressing GlcAT mRNAs and the HNK-1 carbohydrate at high levels might provide the carbohydrate to the Cu and the Gr. These nuclei connect with the ventroposterial thalamic nuclei and the fibers continue to layer IV of the parietal cortex (Waite, 2004). The pathway might, especially, contribute to the strong labeling of HNK-1 in layer IV of GlcAT-P-deficient mice (IV; Fig. 3D).

Concerning the cerebellar system, the precerebellar nuclei (Ruigrok, 2004) showed very strong HNK-1 staining in both wild-type and GlcAT-P-deficient mice. While the pontine nuclei (Pn; Figs. 2B-c, g, l, and p) including the reticulotegmental nucleus (RtTg; Figs. 2B-c and l) expressed moderate signals of the GlcAT transcripts (Figs. 1j and u), the IO and the LRt expressed weak ones (Figs. 1h and s). As afferents to the Pn generally arise from layer V neurons of the ipsilateral cortices, where GlcAT mRNAs and the HNK-1 carbohydrate are expressed, the HNK-1 carbohydrate might be supplied more from layer V to the Pn. The fact that afferent pathways to the IO mainly arise from somatosensory nuclei, such as the spinal trigeminal nucleus and the dorsal column nuclei, where HNK-1 was expressed very strongly, is in accord with the finding that the IO showed diffuse HNK-1 staining. Efferent fibers of the IO are the sole source of cerebellar climbing fibers and terminate on the dendritic tree of Purkinje cells in the molecular layer, in which Purkinje

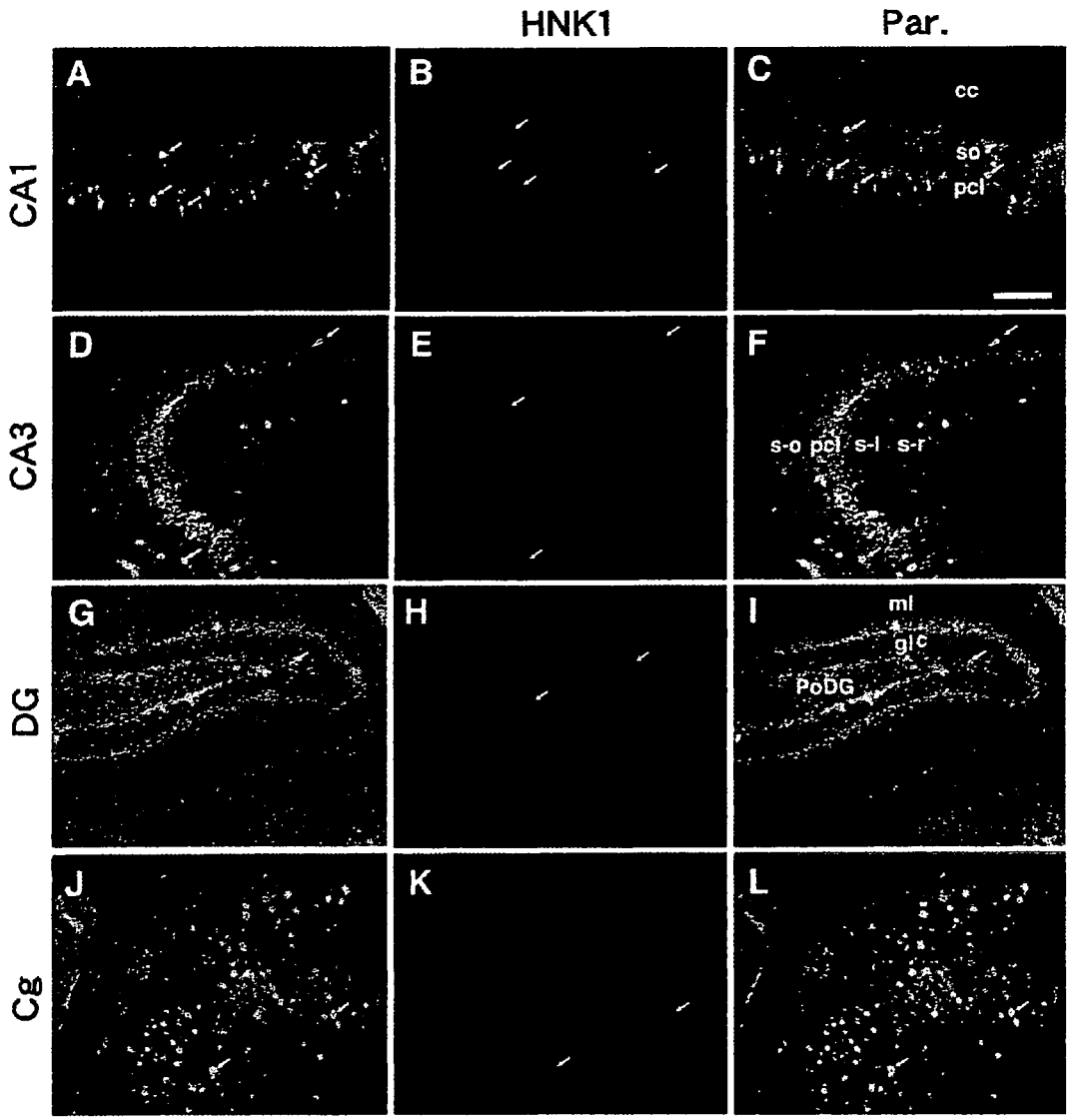


**Fig. 5 – Double-labeled immunofluorescence micrographs with anti-HNK-1 (red) and anti-parvalbumin (green) antibodies in the CA1 subfield (A–C), the CA3 subfield (D–F), the dentate gyrus (G–I), and the cingulated cortex (J–L) of GlcAT-P-deficient mice. Scale bar=300 μm. Arrows show that HNK-1 signals were localized in neuronal cells containing parvalbumin.**

cells expressed GlcAT-P mRNA and then the HNK-1 carbohydrate synthesis was catalyzed and projected to the molecular layer (Figs. 3E and F). Finally, the HNK-1 carbohydrate present in the LRt might have been brought there by fibers that arose from the cerebral cortex, the vestibular nuclei, and the hypothalamus, where GlcAT transcripts were expressed.

As shown in Fig. 2, the HNK-1 carbohydrate epitope widely distributed in most of brain disappeared in the GlcAT-P-deficient mice. However, HNK-1 immunoreactivity remained on neuronal cells in layers III to VI of cerebral cortex in the GlcAT-P-deficient mice (Figs. 2 and 3D). We have already reported that the remaining HNK-1 carbohydrate in the GlcAT-P-deficient mice corresponded to the perineuronal nets (Celio et al., 1998), which are known to comprise lattice-like accumulation of the extracellular matrix on a subset of neurons (Yamamoto et al., 2002). The major extracellur matrix of perineuronal nets are composed of hyaluronan, tenacin-R (Celio and Blumcke, 1994) and chondroitin sulfate proteoglycans such as neurocan, brevican, and phosphacan (Hagihara et al., 1999; Haunso et al., 1999; Matsui et al., 1998; Matthews et al., 2002; Rauch et al., 1991). It should be noted here that HNK-1 carbohydrate is expressed on most of extracellur matrix of perineuronal nets (Brückner et al., 2000). Furthermore, morphological alteration in *Wisteria floribunda* agglutinin (WFA)-labeled perineuronal nets around cortical interneurones in tenascin-R-deficient mice has been reported (Brückner et al., 2000). Then, to examine morphological alteration in *Wisteria*

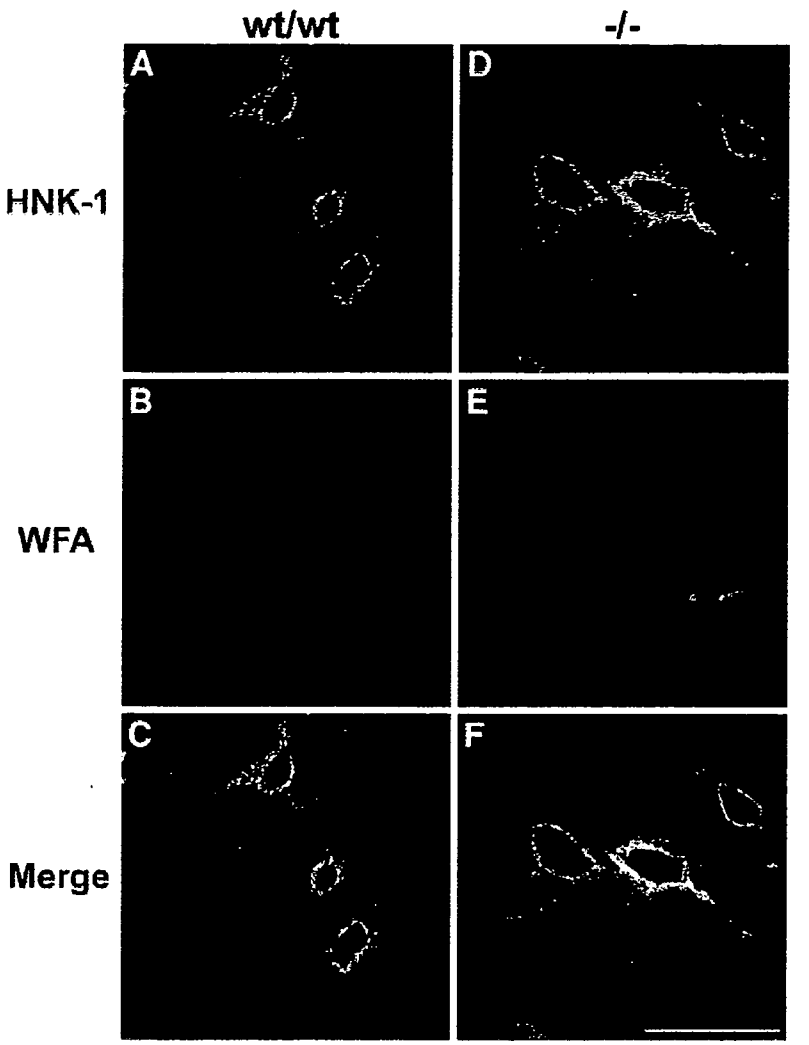


**Fig. 6 – Double fluorescence staining focused on the perineuronal nets with anti-HNK-1 antibody (green) and WFA lectin (red). Brain coronal sections (40 μm thick) from 10-week-old wild-type (wt/wt; A–C) and GlcAT-P-deficient mice (–/–; D–F) were incubated with anti-HNK-1 antibody and WFA (*Wisteria Floribunda* agglutinin) lectin (SIGMA) and then incubated with FITC-conjugated anti-mouse IgM antibodies (zymed) and Rhodamine-conjugated avidin (vector). HNK-1 carbohydrate overlapping perineuronal net was found in GlcAT-P-deficient mice (F) as is the case with wild-type mice (C), and no obvious structural differences of perineuronal nets were observed in GlcAT-P-deficient mice at the fluorescence staining level. Scale bar=50 μm.**

*floribunda* agglutinin (WFA)-labeled perineuronal nets in the GlcAT-P-deficient mice, we carried out double fluorescence staining with the HNK-1 antibody and WFA. As shown in Fig. 6, no obvious structural differences of perineuronal nets were observed in GlcAT-P-deficient mice at the fluorescence staining level, while perineuronal nets show clear structural changes in tenascin-R-deficient mice (Brückner et al., 2000). It suggests that the disappearance of HNK-1 carbohydrate in GlcAT-P-deficient mice has little effect on the formation of perineuronal nets. We are now trying to identify the molecular nature of the HNK-1 carbohydrate remaining in the perineuronal nets in GlcAT-P-deficient mice.

The present study was the first to show the regional relationship between GlcAT transcripts and the HNK-1 carbohydrate as an end-product in the brain, which will be very helpful for investigations of the role of HNK-1 carbohydrate in brain functions. Furthermore, this work provides the first example of histological enzyme-substrate analyses aimed at understanding the glycosylation system in the brain network.

## 4. Experimental procedure

### 4.1. *Animals*

Normal mice (8 weeks old and 45 weeks old, male; C57Bl/6J Jcl from CLEA Japan, Inc., Tokyo, Japan) and GlcAT-P-deficient mice (45 weeks old, male), which were backcrossed with

C57Bl/6J mice for more than eight generations, were utilized for experiments. All procedures were performed according to the guidelines for animal welfare of the Nara Institute of Science and Technology.

### 4.2. *In situ hybridization*

For preparation of riboprobes, the GlcAT-P and GlcAT-S target sequences were amplified using a single preparation of cDNA synthesized from hippocampal total RNA by one round of polymerase chain reaction using the following primers. The size of the final amplification product is shown in parentheses: GlcAT-P, 5'-TAG GGA GTA CTG CAT GTC CG -3'/5'-TAT AGT TGC GTG GTG TCT CT-3' (299 bp: nucleotide Nos. 488–786) and GlcAT-S, 5'-ACG CGC AGC GAG CTG GTG AG-3'/5'-TTT TGG ATT GGA CAA GAT GA-3' (417 bp: nucleotide Nos. 1019–1435). The polymerase chain reaction product was subcloned into pGEM-T easy vector. α $^{35}$S-labeled riboprobes were prepared according to the manufacturer's instructions (Roche Molecular Biochemicals), using *Sal*I and T7 RNA polymerase (T7) for the antisense probe and *Nco*I and SP6 RNA polymerase (SP6) for the sense probe for GlcAT-P; and using *Nco*I and SP6 for the antisense probe and *Sal*I and T7 for the sense probe for GlcAT-S.

*In situ* hybridization histochemistry with [$^{35}$S]-labeled riboprobe ($2\times10^6$ dpm/slide glass) was performed as described previously (Okabe et al., 2001). For tissue preparation, mice were anesthetized with diethyl ether inhalation and decapitated. Coronal sections (14-μm thick) were cut on a cryostat and thaw-mounted onto slides coated with 0.1% 3-aminopropyltriethoxy silane (Sigma-Aldrich, Tokyo, Japan) in acetone. Sections on slides were fixed in 4% formaldehyde in 0.1 M sodium phosphate, pH 7.4, for 20 min at room temperature. Next they were washed, treated with 10 μg/mL protease K in 50 mM Tris–HCl, pH 7.5, and 5 mM EDTA at room temperature for 3 min, postfixed with the above fixative, washed again, acetylated with 24 mM acetic anhydride and 0.1 M triethanolamine for 10 min, washed, then dehydrated through an ascending alcohol series. Each $^{35}$S-labeled riboprobe ($2\times10^6$ dpm/slide glass) was mixed with hybridization buffer; 50% deionized formamide, 0.3 M NaCl, 5 mM EDTA, 10% dextran sulfate, 1× Denhardt's solution, 0.2% N-lauroylsarcosine, 500 μg/mL yeast tRNA, 200 μg/mL salmon testis DNA, 2 mM dithiothreitol and 20 mM Tris–HCl, pH 8.0, placed on the sections, and incubated at 55 °C for 16 h. The sections were washed at 68 °C for 30 min each with 5× NaCl/Cit, 5 mm dithiothreitol and 50% formamide, 2× NaCl/Cit, 5 mm dithiothreitol. And they were treated with 2 μg/mL RNaseA in 0.5 M NaCl, 1 mM EDTA and 10 mM Tris–HCl, pH 7.5, at 37 °C for 30 min, then washed with 50% formamide, 2× NaCl/Cit, and 5 mM dithiothreitol at 68 °C for 30 min and with 2× NaCl/Cit and 0.1× NaCl/Cit at room temperature for 10 min each. After dehydration through an ascending alcohol series and air drying, slides were exposed to imaging plates (BAS2500, Fujifilm, Tokyo, Japan) for 24 h (macro-autoradiogram). The next day, slides were coated with autoradiography emulsion (NTB2, Kodak, Rochester, NY), exposed for 3 weeks, then developed with D-19 developer (Kodak) and fixed with Fuji fix (Fujifilm, Tokyo, Japan, Japan) in distilled water. The sections were observed under a light microscope with dark-field illumination (Nikon Corporation, Tokyo, Japan) (micro-autoradiogram), then sequentially stained with 0.01% thionine acetate (Nacalai Tesque, Inc., Kyoto, Japan) for observation under bright-field illumination. The specificity of the riboprobes was checked by comparing brain sections hybridized with sense and antisense probes. No signals were detected on the adjacent sections incubated in a control hybridization mixture containing sense probes corresponding to GlcAT cRNAs.

### 4.3. *Estimation of the regional distribution in normal mouse brain*

Pseudo color images of brains in macro-autoradiography (BAS2500) were produced using image analysis software (Win Roof v3.3, Mitani Corporation, Osaka Japan) to judge the differential intensity as described previously (Matsuhashi et al., 2003). Visual inspection of emulsion autoradiograms was also used to identify brain nuclei and particular cell types. Definitions for brain regions and nuclei were established following brain maps (Franklin and Paxinos, 1997). A combination analysis of macro- and micro-autoradiograms was used to establish the comparative distribution of the two transcripts, which was presented as a system of pluses (Table 1), with four pluses (++++) indicating maximal signal intensity. The hybridization patterns were virtually indistinguishable between mice ($n=3$) and among independent hybridizations ($\geq 2$).

### 4.4. *Quantification of signal intensity of GlcAT transcripts in the CA3 subfield of the hippocampal formation in microautoradiography*

The signal intensities in sections cut at −2.0 mm with respect to the bregma were examined. The signal intensity within a $\phi$175.25 μm$^2$ circular field in the CA3 subfield under dark-field illumination was measured automatically using Win Roof v3.3 ($n=8$). The raw signal intensity of a circle in the isocortex was taken background in each section. Figs. 4A–D shows representative fields among images used for the analyses.

### 4.5. *Immunohistochemistry*

Mice (45weeks old) were perfused under deep anesthesia through the heart with 4% paraformaldehyde in 0.1 M sodium phosphate, pH 7.4. Brains were removed, kept in the same fixative at 4 °C for 16 h and in 30% sucrose, 0.1 M sodium phosphate, pH 7.4, at 4 °C for 48 h, frozen on dry ice, and sectioned coronally at 30 μm on a cryostat.

Immunohistochemical analysis was performed with mouse monoclonal HNK-1 antibody (American Type Culture Collection) and then the anti-mouse IgM antibody conjugated with horseradish peroxidase (HRP). Sections were developed with 0.02% 3,3'-diaminobenzidine (Wako Pure Chemical Industries, Ltd., Osaka, Japan) in 50 mM Tris–HCl, pH 7.6, 0.6% ammonium nickel (II) sulfate hexahydrate (Wako Pure Chemical Industries), and 0.01% hydrogen peroxide. Images were captured with an Axioplan 2 (Carl Zeiss, Tokyo, Japan). For double-labeled immunofluorescence histochemistry, the sections were incubated with biotinylated HNK-1 antibody and mouse

monoclonal anti-parvalbumin (Swant, 235, Bellinzona, Switzerland) as primary antibodies and then with rhodamine–avidin and anti-mouse IgG antibody conjugated with fluorescein isothiocyanate (BIOSOURCE International, CA, USA) as secondary antibodies. Images were captured with a laser scanning microscope (LSM510 invert; Carl Zeiss, Tokyo, Japan). The immunohistochemical patterns were virtually indistinguishable between mice ($n=3$) and among independent reactions ($\geq 3$).

## Acknowledgments

This work was partly supported by grants from the Ministry of Education, Science, Culture, and Sports (13680843 to K.K.). This work was also supported in part by a Grant-in-Aid for Creative Scientific Research (16GS0313 to S.O.) and a Grant-in-Aid for Scientific Research on Priority Areas (A-14082203 to T.K.) from the Ministry of Education, Culture, Sports and Technology.

## REFERENCES

Brückner, G., Grosche, J., Schmidt, S., Härtig, W., Margolis, R.U., Delpech, B., Seidenbecher, C.I., Czaniera, R., Schachner, M., 2000. Postnatal development of perineuronal nets in wild-type mice and in a mutant deficient in tenascin-R. J. Comp. Neurol. 428, 616–629.

Butcher, L.L., 1995. Cholinergic neurons and networks, In: Paxinos, G. (Ed.), The Rat Nervous System, second edition. Academic Press Inc., San Diego, pp. 1003–1015.

Butcher, L.L., Woolf, N.J., 2004. Cholinergic neurons and networks revisited, In: Paxinos, G. (Ed.), The Rat Nervous System, third edition. Academic Press Inc., San Diego, pp. 1257–1268.

Celio, M.R., Blumcke, I., 1994. Perineuronal nets: a specialized form of extracellular matrix in the adult nervous system. Brain Res. Rev. 19, 128–145.

Celio, M.R., Spreafico, R., Biasi, S., Vitellaro-Zuccarello, L., 1998. Perineuronal nets: past and present. Trends Neurosci. 21, 510–515.

Chou, D.K.H., Ilyas, A.A., Evans, J.E., Costello, C., Quarles, R.H., Jungalwala, F.B., 1986. Structure of sulfated glucuronyl glycolipids in the nervous system reacting with HNK-1 antibody and some IgM paraproteins in neuropathy. J. Biol. Chem. 261, 11717–11725.

Dityatev, A., Schachner, M., 2003. Extracellular matrix molecules and synaptic plasticity. Nat. Rev., Neurosci. 4, 456–468.

Franklin, K.B.J., Paxinos, G., 1997. The Mouse Brain in Stereotaxic Coordinates. Academic Press Inc., San Diego.

Groenewegen, H.J., Witter, M.P., 2004. Thalamus, In: Paxinos, G. (Ed.), The Rat Nervous System, third edition. Academic Press Inc., pp. 407–453.

Hagihara, K., Miura, R., Kosaki, R., Berglund, E., Ranscht, B., Yamaguchi, Y., 1999. Immunohistochemical evidence for the brevicantenascin-R interaction: colocalization in perineuronal nets suggests a physiological role for the interaction in the adult rat brain. J. Comp. Neurol. 410, 256–264.

Haunso, A., Celio, M.R., Margolis, R.K., Menoud, P.A., 1999. Phosphacan immunoreactivity is associated with perineuronal nets around parvalbumin-expressing neurones. Brain Res. 834, 219–222.

Kakuda, S., Sato, Y., Tonoyama, Y., Oka, S., Kawasaki, T., 2005. Different acceptor specificities of two glucuronyltransferases involved in the biosynthesis of HNK-1 carbohydrate. Glycobiology 15, 203–210.

Kosaka, T., Katsumaru, H., Hama, K., Wu, J.Y., Heizmann, C.W., 1987. GABAergic neurons containing the Ca2+-binding protein parvalbumin in the rat hippocampus and dentate gyrus. Brain Res. 419, 119–130.

Kosaka, T., Isogai, K., Barnstable, C.J., Heizmann, C.W., 1990. Monoclonal antibody HNK-1 selectively stains a subpopulation of GABAergic neurons containing the calcium-binding protein parvalbumin in the rat cerebral cortex. Exp. Brain Res. 82, 566–574.

Kosaka, T., Heizmann, C.W., Fujita, S.C., 1992. Monoclonal antibody 473 selectively stains a population of GABAergic neurons containing the calcium-binding protein parvalbumin in the rat cerebral cortex. Exp. Brain Res. 89, 109–114.

Kruse, J., Maihammer, R., Werneche, H., Faissner, A., Sommer, I., Goridis, C., Schachner, M., 1984. Neural cell adhesion molecules and myelin-associated glycoprotein share a common carbohydrate moiety recognized by monoclonal antibodies L2 and HNK-1. Nature 311, 153–155.

Kruse, J., Keilhauer, G., Faissner, A., Timpl, R., Schachner, M., 1985. The J1 glycoprotein—A novel nervous system cell adhesion molecule of the L2/HNK-1 family. Nature 316, 146–148.

Kunemund, V., Jungalwala, F.B., Fischer, G., Chou, D.K., Keilhauer, G., Schachner, M., 1988. The L2/HNK-1 carbohydrate of neural cell adhesion molecules is involved in cell interactions. J. Cell Biol. 106, 213–223.

Malmierca, M.S., Merchán, M.A, 2004. Auditory system, In: Paxinos, G. (Ed.), The Rat Nervous System, third edition. Academic Press Inc., San Diego, pp. 997–1082.

Martini, R., Xin, Y., Schumitz, B., Schachner, M., 1992. The L2/HNK-1 carbohydrate epitope is involved in the preferential outgrowth of motor neuron on ventral roots and motor nerves. Eur. J. Neurosci. 4, 628–639.

Matsuhashi, H., Horii, Y., Kato, K., 2003. Region-specific and epileptogenic-dependent expression of six subtypes of alpha2,3-sialyltransferase in the adult mouse brain. J. Neurochem 84, 53–66.

Matsui, F., Nishizuka, M., Yasuda, Y., Aono, S., Watanabe, E., Oohira, A., 1998. Occurrence of a N-terminal proteolytic fragment of neurocan, not a C-terminal half, in a perineuronal net in the adult rat cerebrum. Brain Res. 790, 45–51.

Matthews, R.T., Kelly, G.M., Zerillo, C.A., Gray, G., Tiemeyer, M., Hockfield, S., 2002. Aggrecan glycoforms contribute to the molecular heterogeneity of perineuronal nets. J. Neurosci. 22, 7536–7547.

Okabe, A., Tawara, Y., Masa, T., Oka, T., Machida, A., Tanaka, T., Matsuhashi, H., Shiosaka, S., Kato, K., 2001. Differential expression of mRNAs for sialyltransferase isoenzymes induced in the hippocampus of mouse following kindled seizures. J. Neurochem. 77, 1185–1197.

Ong, E., Suzuki, M., Belot, F., Yeh, J.C., Franceschini, I., Angata, K., Hindsgaul, O., Fukuda, M., 2002. Biosynthesis of HNK-1 glycans on O-linked oligosaccharides attached to the neural cell adhesion molecule (NCAM): the requirement for core 2 beta 1,6-N-acetylglucosaminyltransferase and the muscle-specific domain in NCAM. J. Biol. Chem. 277, 18182–18190.

Pizzorusso, T., Medini, P., Berardi, N., Chierzi, S., Fawcett, J.W., Maffei, L., 2002. Reactivation of ocular dominance plasticity in the adult visual cortex. Science 298, 1187–1189.

Rauch, U., Gao, P., Janetzko, A., Flaccus, A., Hilgenberg, L., Tekotte, H., Margolis, R.K., Margolis, R.U., 1991. Isolation and characterization of developmentally regulated chondroitin sulfate and chondroitin/keratan sulfate proteoglycans of brain identified with monoclonal antibodies. J. Biol. Chem. 266, 14785–14801.

Rhodes, K.E., Fawcett, J.W., 2004. Chondroitin sulphate proteoglycans: preventing plasticity or protecting the CNS? J. Anat. 204, 33–48.

Risold, P.Y., 2004. The septal region, In: Paxinos, G. (Ed.), The Rat Nervous System, third edition. Academic Press Inc., San Diego, pp. 605–632.

Ruigrok, T.J.H., 2004. Precerebellar nuclei and red nucleus, In: Paxinos, G. (Ed.), The Rat Nervous System, third edition. Academic Press Inc., San Diego, pp. 167–204.

Saghatelyan, A.K., Gorissen, S., Albert, M., Hertlein, B., Schachner, M., Dityatev, A., 2000. The extracellular matrix molecule tenascin-R and its HNK-1 carbohydrate modulate perisomatic inhibition and long-term potentiation in the CA1 region of the hippocampus. Eur. J. Neurosci. 12, 3331–3342.

Seiki, T., Oka, S., Terayama, K., Imiya, K., Kawasaki, T., 1999. Molecular cloning and expression of a second glucuronyltransferase involved in the biosynthesis of the HNK-1 carbohydrate epitope. Biochem. Biophys. Res. Commun. 255, 182–187.

Shimoda, Y., Tajima, Y., Nagase, T., Harii, K., Osumi, N., Sanai, Y., 1999. Cloning and expression of a novel galactoside beta1, 3-glucuronyltransferase involved in the biosynthesis of HNK-1 epitope. J. Biol. Chem. 11, 17115–17122 (Erratum in: J Biol Chem 274, 21490).

Simerly, R.B., 2004. Anatomical substrates of hypothalamic integration, In: Paxinos, G. (Ed.), The Rat Nervous System, third edition. Academic Press Inc., San Diego, pp. 335–368.

Terayama, K., Oka, S., Seiki, T., Miki, Y., Nakamura, A., Kozutsumi, Y., Takio, K., Kawasaki, T., 1997. Cloning and functional expression of a novel glucuronyltransferase involved in the biosynthesis of the carbohydrate epitope HNK-1. Proc. Natl. Acad. Sci. U. S. A. 94, 6093–6098.

Terayama, K., Seiki, T., Nakamura, A., Matsumori, K., Ohta, S., Oka, S., Sugita, M., Kawasaki, T., 1998. Purification and characterization of a glucuronyltransferase involved in the biosynthesis of the HNK-1 epitope on glycoproteins from rat brain. J. Biol. Chem. 273, 30295–30300.

Tracey, D., 2004. Somatosensory system, In: Paxinos, G. (Ed.), The Rat Nervous System, third edition. Academic Press Inc., San Diego, pp. 797–815.

Voshol, H., van-Zuylen, C.W., Orberger, G., Vliegenthart, J.F., Schachner, M., 1996. Structure of the HNK-1 carbohydrate epitope on bovine peripheral myelin glycoprotein P0. J. Biol. Chem. 271, 22957–22960.

Yamamoto, M., Marshall, P., Hemmendinger, L.M., Boyer, A.B., Caviness Jr., V.S, 1988. Distribution of glucuronic acid-and-sulfate-containing glycoproteins in the central nervous system of the adult mouse. Neurosci. Res. 5, 273–298.

Yamamoto, S., Oka, S., Inoue, M., Shimuta, M., Manabe, T., Takahashi, H., Miyamoto, M., Asano, M., Sakagami, J., Sudo, K., Iwakura, Y., Ono, K., Kawasaki, T., 2002. Mice deficient in nervous system-specific carbohydrate epitope HNK-1 exhibit impaired synaptic plasticity and spatial learning. J. Biol. Chem. 277, 27227–27231.

Waite, P.M.E., 2004. Trigeminal sensory system, In: Paxinos, G. (Ed.), The Rat Nervous System, third edition. Academic Press Inc., San Diego, pp. 817–851.

Zamze, S., Wing, D.R., Wormald, M.R., Hunter, A.P., Dwek, R.A., Harvey, D.J., 2001. A family of novel, acidic N-glycans in Bowes melanoma tissue plasminogen activator have L2/HNK-1-bearing antennae, many with sulfation of the fucosylated chitobiose core. Eur. J. Biochem. 268, 4063–4078.

MINIREVIEW

Trends in Glycoscience and Glycotechnology
Vol.19 No.106 (March 2007) pp.99–112

# Glycobiological Approach to Understanding Neural Plasticity

## 神経の可塑性における糖鎖の役割

**Kato, Keiko**

Department of Structural and Functional Biosciences for Animals, Graduate School of Life and Environmental Sciences, Osaka Prefecture University1-1 Gakuen-cho, Nakaku, Sakai, Osaka, 599-8531, Japan
FAX: 81-72254-9496 E-mail: kato@vet.osakafu-u.ac.jp

***Key Words***: *neural plasticity, synaptic plasticity, carbohydrate*

**Abstract**

Neural plasticity is necessary for the expression and maintenance of higher brain functions. While most of the experimental approach to the plasticity still remains phenomenalism, analyses at the molecular level have gradually progressed, especially concerning synaptic plasticity. The analyses revealed that several carbohydrate structures play important roles in the synaptic plasticity. This review describes the roles of 5 of these species of carbohydrates.

要　約

神経の可塑的変化は、脳の高次機能の発現と維持に必須の反応であるが、ほとんどの可塑的変化は、いまだ現象論に留まっている。その中において、海馬を中心としたシナプス可塑性については、ずいぶんと分子レベルの解析が進んできており、特定の糖鎖構造が重要な役割を演じていることが明らかとなってきた。そこで本稿では、5種の糖鎖構造に焦点を絞り、シナプス可塑性への関わりについて解説する。

### A. Introduction

The brain comprises a sensory system, a motor system, a limbic system for learning and memory, and a homeostasis system related to body temperature and reproduction. These systems communicate with each other via a complex neural network to express higher brain functions. The neural circuitry is not complete throughout life, with the addition, revision, and maintenance of information over long periods causing the network to change. Such phenomena are known collectively as neural plasticity, comparable to the plasticity of clay. Neural plasticity occurs in various neural regions during (i) development of the neural circuitry in the fetus, (ii) physical and mental development in children, (iii) learning and memory, (iv) breeding, and (v) regeneration following neural degeneration. Several representative examples involving the auditory system are described.

Research has progressed psychophysically concerning the discrimination of frequency, loudness, pitch, tone, and source localization of sound, and it has recently been revealed that the acquirement of source localization, at least is related with neural plasticity. When spectacles were embedded in the optic tectum of juvenile barn owls, the auditory space map in the external nucleus of the inferior colliculus shifted according to the optic displacement of the prisms and induced changes in interaural timing difference (ITD), one of the most important cues for sound localization. After adapting the owls with a prism in the optic tectum, ITD tuning shifted to a long time ($\mu$s). Removing the prism after adaptation led to the tuning returning to normal, short time. Embedding

### A. 序　論

脳は、感覚系、運動系、学習記憶に代表される辺縁系そして、体温や生殖に関係した生体調節系、に分類することができるが、実際には、これらの系（システム）は、複雑に入り組んだ神経回路網によりお互い連絡し、中枢としての脳の高次機能を発現する。この神経回路網は、厳密には完成された形というものはなく、記憶・学習に代表されるように、長期にわたる持続的な情報が加算され保持されることにより、新たな回路が形成・維持され、時に変化し、修正されるものである。こうした神経回路に生じる現象を粘土細工にたとえて、“神経が可塑性を獲得する”という。そして様々な神経の可塑的変化は、(i) 発生過程を含む、脳の回路発達時、(ii) 成長期における心身の発達時期、(iii) 学習記憶時、(iv) 繁殖期、そして (v) 神経損傷に伴う再生時に、様々な神経領域で生じることがわかってきた。では、具体的にどの様な現象が存在するのか、ここでは聴覚系を例に挙げて幾つか記述する。

これまで、音の周波数、音の大きさ・高さ、音色の識別、音源定位（どこから音が聞こえるか）の獲得について、心理物理学的に研究が進められてきたが、近年の神経科学の進歩により、少なくとも音源定位が神経可塑性に関わることがわかってきた。メンフクロウの幼鳥脳の視蓋にプリズムを埋め込み、視覚に変化を起こすと、視覚と聴覚の知覚にずれが生じ、音源定位の手がかりのひとつ、両耳間時間差（ITD）が変化する。プリズムで適応させた幼鳥から、いったんプリズムをはずすと、ITDは短縮するが、再びプリズムを埋め込むと、当初埋め込んでいた時の時間差に戻る。すなわち、メンフクロウは、幼鳥の発達時に得たプリズム適応を保持（記憶）していたこ

the prism again led to a shift of ITD tuning as when the prism was first embedded. This showed that juvenile owls memorize prism adaptation acquired developmentally (1,2). The sensitive period of the prism adaptation ends as the owls approach sexual maturity, at about 200-250 days old, which suggests that acquirement of sound localization is a neural plasticity occurring in the developmental period. For lots of neural plasticity containing developments of auditory, visual, and motor systems as well as sound localization, the periods required for the acquirement are determined and called critical periods. For example, birds communicate through various songs. Song learning involves two components: song memorization and vocal learning. Juvenile birds memorize songs early in life during a critical period and birds are able to sing by vocal learning following the end of the critical period (3). While the start and termination of critical periods seem to be programmed by genetic information, the molecular mechanisms are little understood.

As an example of adult neural plasticity, nonreproductive female midshipman fish present no response to male vocalizations by the inner ear. However, nonreproductive female treated with testosterone or 17β-estradiol exhibit an increase in the degree of temporal encoding of the frequency content of male vocalizations by the inner ear that mimics the reproductive female's auditory phenotype(4). Furthermore, the response of the inner ear is observed seasonally in the summer but not in the winter (5) and is understood as a neural plasticity in breeding season.

Other examples of adult neural plasticity involve neural diseases. For example, it is known that synapses form and neurites develop following brain ischemia and trauma. In addition, neural stem cells in the olfactory ventricle, the lateral ventricle, and the subgranule cell layer of the dentate gyrus develop as new neural cells, which are involved in regeneration. In addition, epilepsy is a disease involving abnormal neural plasticity and repetitive seizures caused by the overloaded discharge of neuronal cells. Finally, there have been reports concerning adult neural plasticity caused by neural diseases.

Neural plasticity is evaluated based on morphological and physiological observations at cell biological level. So far, the synaptic plasticity existing between neurons and between neurons and effector cells has been extensively investigated. It is thought that the physiological activity in neural circuits reacts and changes depending on the condition of synapses. Based on the notion that "two synaptically coupled neurons wire together more strongly, when neurons can fire and fire together (paraphrase of Hebb's postulation 1994)", the molecular cascade and signal transmission in the synaptic region lead to neural plasticity *in vivo* and this has been investigated with a focus on the hippocampus (6,7). For

とになる (1、2)。このプリズム適応は、生後 200-250 日齢に成長したフクロウには起こらない。この日齢は性成熟期に当たることから、音源定位の獲得は子供の時期におこる、神経の可塑的変化であることがわかる。この音源定位に代表されるように、聴覚、視覚、運動発達等に含まれる幾つかの能力は、神経可塑性の獲得時期が決まっており、その時期を臨界期という。例えば鳥は様々なさえずりでコミュニケーションをおこなっているが、臨界期に当たる時期に歌を聴き覚えるが、臨界期を過ぎると、歌を覚えることができない。その一方、さえずりの練習（学習）は臨界期を過ぎていても、学習が成り立ち、うまく歌えるようになる(3)。こうした臨界期のスタートや終了時期の決定は、それぞれ遺伝子情報にプログラムされていると考えられるが、その分子メカニズムは、今のところほとんどわかっておらず、今後の解析に期待される。

次に成熟後に神経可塑性を獲得する例として、不妊雌魚の内耳からの電気信号は、雄の求愛の発声周波数に反応しないが、この不妊雌魚にテストステロンや１７βエストラジオールを与えたところ、内耳は反応し、生殖能力をもつ雌の聴覚表現型を示すようになったという報告がある (4)。またこの内耳の反応は、夏にのみ観察され、冬には消失することから (5)、繁殖期に関連した神経可塑性である事が知られている。

さらに、成熟後に神経可塑性を獲得する別の例として、疾患に関わる可塑的変化も挙げられる。例えば、脳虚血や外傷等により神経損傷を受けた後、新たに軸索をのばし、シナプス結合を形成することが知られている。また、嗅脳室、側脳室、及び海馬歯状回下顆粒細胞層に存在する神経幹細胞が、新たな神経細胞へと分化し、再生に関与することも、可塑性の獲得としてとらえられている。またてんかんは、脳虚血や外傷を含む様々な原因がもとになり、異常な神経の可塑的変化を遂げた結果、神経細胞の過剰な放電に由来する反復性の発作を生じる疾患であり、このように脳の疾患が原因で生じる神経の可塑的変化も多く報告されている。

次に細胞生物学的な見方をすれば、神経可塑性は、形態学的及び生理学的な観察に基づき判定される。そして今日まで、特に、ニューロン間あるいはニューロン－効果器細胞間に存在するシナプスの可塑性に注目した解析が行われてきた（シナプス可塑性)。これまで、神経回路網内での活動は、シナプス結合の活動状況に応じて反応し変化すると考えられている。そして「シナプス結合を示すニューロン間は、発火強度に応じて、シナプス結合をさらに強める（Hebb 則の意訳 1994 年)」という考えを基に、シナプス結合部位での信号伝達や分子カスケードが、神経の可塑的変化をもたらすと考え、記憶の中枢といわれる海馬を中心に研究が進められてきた (6、7)。例え

example, when two stimuli (paired pulses) are applied to the presynaptic nerve, paired-pulse facilitation and paired-pulse depression develop according to differences in the timing of the stimuli (2) (short-term synaptic plasticity). Then, in stimuli, frequency of firing in addition to timing seem to induce long-term synaptic plasticity, that is, in synapses in pyramidal cells of the hippocampus and cerebral cortex, high-frequency continuous spike stimuli at ca. 100 Hz and 1sec induce long-term potentiation (LTP) whereas low frequency ones at ca. 1Hz for 10 min induce long-term depression (LTD). Because the periods of continuous activity increase from seconds to hours, LTP and LTD are models for learning and memory. Furthermore, it has been reported that the size of the spine was increased by LTP and reduced by LTD (8,9). Recently, the study of the molecular mechanisms related to synaptic plasticity has progressed, with reports of the involvement of carbohydrates. This review describes recent findings on synaptic plasticity focusing on the hippocampus, one of the regions of the brain that have been analyzed extensively at the molecular level. First, it describes the "mechanisms of hippocampal LTP" and then the involvement of 5 species of carbohydrates in synaptic plasticity.

**B. Mechanisms of Hippocampal LTP**

The hippocampal formation, the center of memory, is linked by unidirectional projections [entorhinal cortex (EC) → dentate gyrus (DG) → CA3 → CA1 → subiculum]. Projections from the entorhinal cortex to the dentate gyrus, from the dentate gyrus to the CA3 subfield, and from the CA3 subfield to the CA1 subfield are known as the perforant-pathway, mossy fibers, and Shaffer collaterals, respectively. Stimuli of the perforant-pathway, mossy fibers, and Shaffer collaterals are recorded in dendrites of granule cells in the dentate gyrus (EC-DG synapse), in the pyramidal cell layer of the CA3 subfield (DG-CA3 synapse), and in the pyramidal cell layer of the CA1 subfield (CA3-CA1 synapse), respectively (10) (Fig. 1). In 1973, Bliss *et al* reported that the response of granule cells in the dentate gyrus to stimulation of the perforant-pathway with high frequency continuous spike stimuli was an induction of LTP for at least 6 hours, in the hippocampus in anesthetized rabbits (11). Then, stimulation of the perforant-pathway was recorded in the dentate gyrus of the hippocampus in un-anesthetized rabbits, resulting in LTP lasting 3 days (12). These results in rabbits indicate that LTP is a model of learning and memory in the hippocampus. Then, the development of a physiological technique with hippocampal slices led to numerous reports of the detection of LTP in DG-CA3 and CA3-CA1 synapses (13), which recently have been more frequent than those with EC-DG synapses. More recently, LTP has been detected in the cerebellum, amygdala, cerebral cortex, and so on.

ば、シナプス前ニューロンに2回刺激を与えた場合(短期シナプス可塑性)、2回の刺激間の時間差に応じて、シナプス後ニューロンの反応が増強する場合(paired-pulse facilitation)と、減衰する場合(paired-pulse depression)がある(2)。この時間差に加えて、発火率の異なる刺激を入力することにより、長期シナプス可塑性が誘導される。海馬や大脳皮質錐体細胞のシナプスなどは、100Hz程度の高頻度連続スパイク刺激を1秒間送ると、長期増強(LTP)が誘導され、1Hz程度の低頻度刺激を10分送ると、長期抑圧(LTD)が起こる。これらの反応持続時間が、短期シナプス可塑性の秒単位から、時間単位に延長することから、記憶学習のモデルとして広く利用されている。さらに、LTPに伴い、後シナプスに位置するスパインが肥大する例や、逆にLTDに伴いスパインが矮小化する例が報告されている(8,9)。近年、こうしたシナプス可塑性に関わる分子メカニズムの解明が進んでおり、糖鎖の関与を示唆する報告も多い。そこで本稿では、シナプス可塑性について、最も分子レベルの解明が進んでいるひとつである海馬を中心に，最近の知見を踏まえて解説する。まずは，海馬LTP発生機序について簡単に解説し、その後構造が特定されている糖鎖のシナプス可塑性への関与について、解説する．

B. 海馬LTP発生機序

記憶の中枢と呼ばれる海馬は、神経回路の方向が一方向であり、皮質内嗅領(EC)→歯状回(DG)→CA3→CA1→海馬支脚へと刺激が伝わる。そして皮質内嗅領から歯状回へ、歯状回からCA3へ、そしてCA3からCA1へと投射される繊維連絡を、それぞれ貫通繊維路(perforant-pathway), 苔状繊維(mossy fiber), シャファー側枝(Shaffer collateral)という。そして、貫通繊維路，苔状繊維，シャファー側枝に刺激を与えると、それぞれ、歯状回顆粒細胞の樹状突起が位置する分子層(EC-DGシナプス)、CA3錐体細胞層（DG-CA3シナプス)、CA1錐体細胞層(CA3-CA1シナプス)から神経活動の記録を得ることができる(10)(図1)。1973年にBlissらが、麻酔を施したウサギ海馬の貫通繊維路を高頻度刺激し、投射先の歯状回・顆粒細胞樹状突起で記録をとったところ、少なくとも6時間の持続した電位の上昇を観察した。これは、貫通繊維路(軸索)と顆粒細胞樹状突起間でのシナプスにおける長期増強を最初に見たものである(11)。その後無麻酔下のウサギを用いた試みでは、3日間LTPが持続したことから、LTPは海馬における記憶のモデルとしてとらえられるようになった(12)。その後、海馬スライスを利用した電気生理学的な計測の容易さも手伝って、苔状繊維とCA3錐体細胞樹状突起間（DG-CA3）シナプスや、シャファー側枝とCA1錐体細胞樹状突起間(CA3-CA1)シナプスにおいて、LTPが観察されるようになり(13)、今では貫通繊維路より利用される頻度が高くなっている。さらに最近では、小脳、大脳皮質、扁桃体等様々な脳領域でLTPの現象が見つかっており、今では、海馬特有の反応であるというよりは、もう少し一般化したモデルとしてとらえられるようになった。

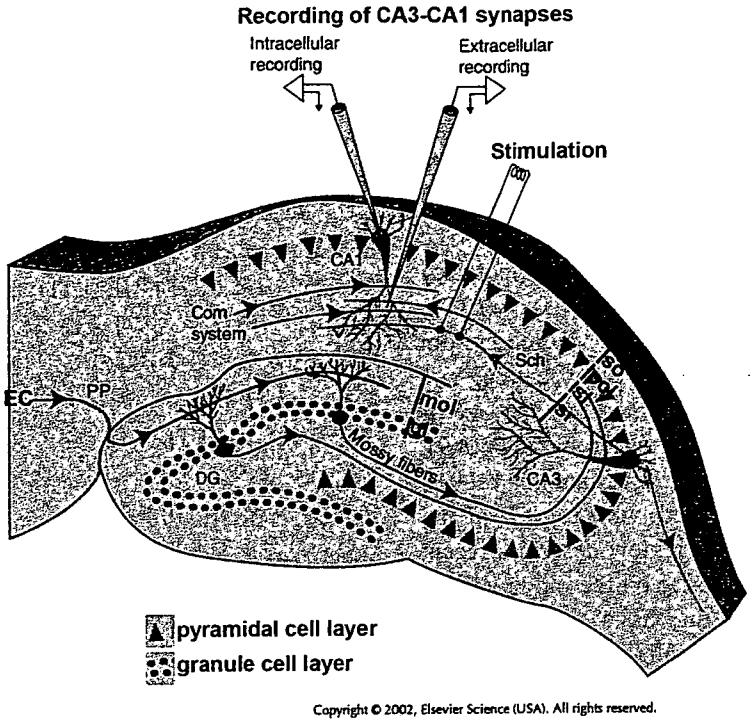




**Fig. 1. A picture of a transverse hippocampal brain slice prepared from the rat and mouse, which was modified slightly from a fig in Fundamental Neuroscience 2nd ed[2]. Com system, commissural system; DG, dentate gyrus; EC, entorhinal cortex; gl, granule cell layer; mol, molecular layer; pcl, pyramidal cell layer; PP, perforant-pathway; Sch, schaffer collateral; sl, stratum lucidum; so stratum oriens; sr, stratum radiatum.**

Next, this review describes the molecular mechanisms of LTP simply. The induction of LTP depends on an increase in the intracellular concentration of calcium ions ($[Ca^{+2}]i$) in some key compartment of pre- and/or postsynaptic cells. The regulation of $[Ca^{+2}]i$ for induction of LTP is controlled by four pathways that have been well studied: *N*-methyl-*D*-aspartate receptor (NMDAR); α-amino-3-hydroxy-5-methyl-4-isoxazole propionic acid receptor (AMPAR); calcium influx through voltage-gated calcium channels (VGCCs); and the release of calcium from intracellular stores. The receptors were located in the spine and dendritic shaft (7,14).

While the AMPAR has relatively low $Ca^{+2}$ permeability and AMPAR-mediated conductance is essentially voltage-independent, the NMDAR becomes permeable to $Ca^{+2}$ with the lifting of the $Mg^{2+}$ block but this channel block is relieved by sufficient depolarization of the postsynaptic membrane. Thus, the NMDA-mediated conductance is dependent on voltage. After enough postsynaptic depolarization induces the release of $Mg^{2+}$ from NMDAR, the glutamate released from pre-synapses binds to the NMDAR and causes an influx of $Ca^{+2}$ into dendritic spines on the postsynaptic cell. The $[Ca^{+2}]i$ that increased is thought to activate CaM kinase II ($Ca^{2+}$-dependent

次に、LTP の分子機構について簡単に解説する。LTP の誘導には、前及び後シナプスの細胞内カルシウム濃度 ($[Ca^{+2}]i$) の上昇が必須である。後シナプスへのカルシウムの流入方法は、NMDA 受容体 (NMDAR, N-methyl-D-aspartate receptor); AMPA 受容体 (AMPAR, α -amino-3-hydroxy-5-methyl4-isoxazole receptor); 電位依存的カルシウムチャネル (VGCCs)；細胞内カルシウムストアを介する事が知られており、これら受容体は後シナプスの位置するスパインや樹状突起軸に分布している (7、14)。

AMPAR が $Ca^{+2}$ に対する透過性が低く、電位依存性伝導を示さない受容体であるのに対して、NMDAR は通常 $Mg^{+2}$ により開口がブロックされており $Ca^{+2}$ を透過しない、電位依存性伝導を示す受容体である。グルタミン酸による AMPAR の開口による $Ca^{+2}$ 流入により、後シナプス膜が十分に脱分極すると、NMDAR から $Mg^{+2}$ が離れて、チャネルが開口する。この NMDAR のチャネルの開口と、前シナプスからの $Ca^{+2}$ 放出とが一致したときのみ、$Ca^{+2}$ が後シナプスへ流入する。増加した $[Ca^{+2}]i$ が、スパイン直下の CaM kinase II ($Ca^{2+}$-dependent kinase II) 等のカルシウム依存性のキナーゼを活性化し、その

kinase II), which plays a key role in the induction of LTP. While this progress is known as NMDAR-dependent LTP, LTP not requiring the NMDAR also exists (NMDA-independent LTP) (15-17). For example, in the presence of the competitive antagonist APV (2-amino-5-phosphnovalerate), LTP has been induced in DG-CA3 synapses. The NMDA-independent LTP has been prevented by a blocker of VGCC, showing that VGCC is involved in the induction of LTP instead of NMDAR (15,16,18). Also, it is known that NMDA-independent LTP occurs via VGCC in some of the CA3-CA1 synapses.

Another mechanism for the induction of LTP involves the metabotropic glutamate receptor (mGluR) (19). Induction of LTP was prevented by a blocker of mGluR, MCPG [(+)-α-methyl-4-carboxy-phenylglycine], in the CA3-CA1 synapse, while LTP was induced by addition of MCPG following highly frequent stimulation. This indicates that mGluR functioned in the pre-synapse. Concerning the mechanism of $Ca^{2+}$ release from intracellular stores dependent on mGluR, the glutamate released by highly frequent stimulation activates PLC (phospholipase C) via mGluR and PLC enzymatically breaks down membrane phospholipids to form DAG (diacylglycerol) and $IP_3$ (inositol 1,4,5-trisphosphate). DAG modulates channel activity through PKC (protein kinase C) and $IP_3$ mobilizes the increase of $[Ca^{+2}]i$ from intracellular stores. The increase in $[Ca^{+2}]i$ does not occur as quickly as the opening of VGCCs. Finally, PKC via mGluR and CaM kinase via NMDAR seem to play important roles in the maintenance of LTP. Additionally, CREB phosphorylated by PKA (protein kinase A) and MAP kinase is also important to maintain LTP (2). However, there is no unified view regarding the molecular mechanisms of LTP's induction, while numerous works at molecular level have been reported. Therefore, further research into these molecular mechanisms in addition to the involvement of carbohydrates is needed.

Some forms of LTD appear to be mediated by the NMDAR and the VGCCs and seem to result from depotentiation. It was suggested that a low $[Ca^{+2}]i$ activates a protein phosphatase and then causes LTD, while a high $[Ca^{+2}]i$ causes LTP (21). A recent report suggested that inhibition of VGCCs in presynapses induces LTD in interneuronal synapses in the mossy fiber-stratum lucidum (21). Finally, progress in the molecular study of LTD is also expected in the future.

### C. Polysialic Acid

PSA (Polysialic acid) is a post-translational modification consisting of a homopolymer of α2,8-linked sialic acids present in the cell membrane. In the brain, PSA is found in a limited number of glycoproteins and predominantly on the neural cell adhesion molecule (NCAM) and sodium channel α subunit (22,23). While research has so far been more frequent concerning PSA-NCAM, concerning the PSA

後の細胞内カスケードにより、LTPが生じると考えられている。一方で、このようなNMDARを介した$Ca^{+2}$流入により誘導されるLTP (NMDAR-dependent LTP) とは異なる、NMDARを介さないLTPの誘導も存在する（15–17)。例えば苔状繊維-CA3錐体細胞間シナプスは、NMDAR阻害剤であるAPV(2-amino-5-phosphonovalerate)存在下で、LTPを発現する。この時、APVと共にVGCC阻害剤を与えることにより、LTPが消失することから、NMDARの代わりにVGCCが、LTPの誘導に関与することがわかる(15、16、18)。NMDAR-dependent LTPが多くを占めるCA3-CA1シナプスにおいても、一部VGCCが、LTPの誘導に関与することが知られている。

加えて，代謝型グルタミン酸受容体(mGluR, metabotropic glutamate receptor)も細胞内カルシウム濃度の上昇に関与することが知られている(19)。代謝型グルタミン酸受容体は，後シナプスだけでなく前シナプスにも存在する。例えばCA3-CA1シナプスにおいて、mGluRの拮抗剤であるMCPG [(+)- α -methyl-4-carboxy-phenylglycine]を投与した後、高頻度刺激(high-frequency stuimulation)を与えると、LTPの誘導が抑制される。その一方で、高頻度刺激を与えた後にMCPGを投与した場合は、LTPの誘導がおこる。これは、mGluRが前シナプスにおいて作用したことを示している（19)。mGluRのカルシウム放出に関わる分子メカニズムについては、高頻度刺激により放出されたグルタミン酸が、mGluRを介してPLC (phospholipase C)を活性化し，PLCが膜上のリン脂質をDAG (diacylglycerol)と$IP_3$ (inositol 1,4,5-trisphosphate)に分解後，DAGがPKC（protein kinase C）を介してチャネルを活性化し、$IP_3$が細胞内カルシウム濃度の亢進をになうようである。mGluRを介したカルシウムの放出は，カルシウムチャネルを介した反応に比べゆっくりしたものであることからも，mGluRを介したPKCは、先に述べたNMDARを介したCAM kinaseと共にLTPの維持に重要な役割を演じるようである。さらに、長期増強の維持に，protein kinase A (PKA), MAP kinaseによりリン酸化を受けるCREBの転写活性の亢進も必要であると考えられている(2)。しかしながらLTP誘導の分子機構は、いまだ多くの点で共通の見解が得られていない事が多く、糖鎖の関与と共に今後のさらなる研究の進展が期待される。

LTDもLTPと同様，NMDARやVGCCsの関与が示唆されているが，細胞内カルシウム濃度のちがいにより，その後のシグナル系の変化がLTDの誘導に関与しているようである(20)。最近の論文では、苔状繊維 - 透明層 (stratum lucidum)における介在ニューロン (interneuron) シナプスでは、前シナプスの電位依存性$Ca^{+2}$チャネルの抑制が、LTDを誘導する事例が報告されており(21)、LTDの分子機構についても、今後の研究の進展が期待される。

### C. ポリシアル酸 (PSA)

ポリシアル酸は、α -2,8結合したシアル酸の直鎖状ポリマーからなる細胞表面糖鎖であり、脳でのポリシアル酸修飾を受ける担体糖タンパク質として、神経細胞接着分子(NCAM)と膜電位依存性ナトリウムチャネルαサブユニットが知られている（22、23)。PSA-NCAMが、最もシナプス可塑性について研究が進んでいる。その一方で、ナトリウムチャネルαサブ

in the sodium channel α subunit, researches have focused on the involvement of sialic acids with channel activity (24). Therefore, this review mainly describes PSA-NCAM.

NCAM is expressed on the membranes of neurons and glia cells and is an adhesion molecule that promotes cell-cell interaction with homophilic binding. NCAM is classified by its type of cytoplasmic domain into NCAM-120 [glycosylp hosphatidylinositol (GPI) anchor type], NCAM-140 [short cytoplasmic domain], and NCAM-180 [long cytoplasmic domain]. Only NCAM-180 contains PSA. Two related enzymes: ST8Sia II (STX) and ST8Sia IV (PST), are responsible for the polymerization of sialic acid in α2 → 8 linkages in the fifth Ig (immunoglobulin)-like domain of the extracellular domain (25–27). *In vitro* analysis has suggested that ST8Sia IV has greater polymerizing activity than ST8Sia II and the coexistence of these enzymes increases the activity (28).

In polysialylated-NCAM, ionic repulsion caused by the cationic charge of polysialic acid on NCAM is an impediment to membrane-membrane contact (29) and increases elasticity structurally, leading to an increase of neural plasticity. Concrete examples include the outgrowth of neurites and axons and structural changes of synapses (30–34). Furthermore, several experimental approaches: treatment with Endo-N (endoneuraminidase) and mice deficient in ST8Sia II, ST8Sia IV, and NCAM, have revealed roles of PSA-NCAM in synaptic plasticity. Therefore, this review focuses on the function of PSA in synaptic plasticity.

First, it explains the distribution of PSA and NCAM in the hippocampus according to the unidirectional connection described in "Mechanisms of hippocampal LTP" (Fig. 1). Immunoelectron microscopy with anti-NCAM-180 antibody demonstrated that about one-third of the postsynaptic density expresses PSA-NCAM in the molecular layer of the dentate gyrus receiving the perforant pathway (35). The ratio of one-third obtained with anti-NCAM-180 antibody is consistent with that obtained with anti-PSA antibody (36,37). On the other hand, PSA and NCAM also seem to occur in the presynaptic membrane independently. While NCAM is expressed in the mossy fiber bundles and boutons, PSA is distributed in unmyelinated axons with the mossy fiber bundles and immature boutons. These results show that not all NCAM is modified with PSA (33, 38). Additionally, there was no expression of either NCAM or PSA in the DG-CA3 synapse receiving the mossy fiber (36). Finally, axons on the Schaffer collateral and pre- and post-synaptic membranes in the CA1 pyramidal layer are PSA-positive, which seems to show PSA-NCAM-positivity, because the PSA in the Schaffer collateral disappears in NCAM-deficient mice (39). Referring to this distribution, the involvement of PSA-NCAM in synaptic plasticity is described below.

ユニットにおける、シアル酸修飾とチャネル活性の関連性についての研究は、骨格筋あるいは心筋のナトリウムチャネルに注目した研究が中心であることから(24)、本稿ではPSA-NCAMについて解説する。NCAMは、ニューロンやグリア細胞膜上で発現し、そのホモフィリックな結合により細胞間相互作用を促進する、細胞接着因子である。NCAMは、細胞質ドメインのちがいにより、NCAM-120[GPI(glycosylphosphatidylinositol)アンカータイプ], NCAM-140 [short cytoplasmic domain], NCAM-180 [long cytoplasmic domain]に分けられ、NCAM-180のみ、ポリシアル酸化を受ける。これは，NCAM細胞外ドメイン上の第5Ig (immunoglobulin)様ドメインにあらかじめ付加されたN結合型糖鎖末端のシアル酸が，ST8Sia II (STX)とST8Sia IV (PST)により，α2→8結合シアル酸重合を受けるものである(25–27)。これら2種の酵素活性については、共に直鎖状のポリシアル酸にシアル酸を転移し、ST8Sia IIよりもST8Sia IVの方が重合活性が高く、さらにST8Sia IIとST8Sia IV共存時が最も重合活性の高いことが*in vitro*の実験系より証明されている(28)。

ポリシアル酸化されたNCAM-180は、ポリシアル酸の負電荷による反発により、NCAM本来の細胞間相互作用の能力を消失し(29)、構造学的に融通性を亢進し、可塑性を高めるようである。具体的には，神経発生の時期における突起伸展や軸索の伸長、さらにはシナプスの構造変化を示す報告がある(30–34)。さらに、PSAを分解するEndo-N(endoneuraminidase)を利用した研究に加え、NCAM, ST8Sia IIそしてST8Sia IVのノックアウトマウスが作成されたことから、シナプス可塑性へのPSAとNCAMの役割がずいぶん明らかになってきた。

まずは、海馬内における発現分布を、「海馬LTP発生機序」の項で記した海馬内繊維連絡に従って記す(図1)。まずPSA-NCAMは、貫通繊維路が投入される海馬歯状回分子層に分布する後シナプス肥厚のおおよそ1/3に発現している(35)。この1/3という比率は、抗PSA抗体(735 mAb, MenB mAb)及び抗NCAM-180抗体を用いた免疫電顕により同様の結果を得ていることから、PSA-NCAMの存在を表していると考えられる(36,37)。一方で、PSAとNCAMそれぞれは、後シナプス肥厚だけでなく一部の前シナプス膜にも存在することから、前シナプス膜におけるPSAの担体については疑問が残る。次に、苔状繊維においては、NCAMが、苔状繊維束及び投射先であるCA3領域内の神経終末に分布する。その一方でPSAは、苔状繊維束のうちミエリン梢を巻いていない軸索と、未分化な一部の神経終末に分布しており、すべてのNCAMがPSA-NCAMではないことを示している(33,38)。さらに、苔状繊維の投射によるDG-CA3シナプスにはNCAM及びPSAは共に存在しないようである(36)。最後に、シャファー側枝については、シャファー側枝に当たる軸索及びCA1領域に存在するCA3-CA1シナプスの前シナプス膜及び後シナプス膜共にPSA陽性であった。このシャファー側枝におけるPSA分布は、NCAM欠失ノックアウトマウスでは陰性であったことから、PSA-NCAMの分布を示していると考えられる(39)。以上のPSA-NCAMの分布を参考に、以下にPSAとシナプス可塑

**Table. I. Roles of polysialic acid and NCAM in neural development and synaptic plasticity.** This table was modified from two tables in Ref 42,43, and 44. – indicates impairment of function; + indicates normal function. n.d., not detected; n.d.*, there might be no difference; $ shows that impairment was rescued by elevation of extracellular $Ca^{2+}$ concentrations from 1.5 to 2.5 mM; # shows impairment in the adult but not juvenile.

| Function | Endo-N | NCAM-/- | conditional NCAM-/- | ST8Sia IV-/- | ST8Sia II-/- | Molecular basis |
|---|---|---|---|---|---|---|
| Migration of neural precursors | –[43,50] | –[43,51,52] | n.d.* | +[43] | +[42] | PSA-dependent NCAM function |
| Lamination of mossy fibers | –[33] | –[41] | +[44] | +[43] | –[42] | ST8Sia II-dependent PSA-NCAM function |
| STP in CA3-CA1 synapse | –[34,39] | –[39] | +[44] | +[43] | +[42] | PSA-dependent NCAM function |
| STP in DG-CA3 synapse | +[42] | +[41] | +[44] | +[43] | +[42] | No effect of PSA or NCAM |
| STP in EC-DG synapse | n.d. | –[40] | n.d. | +[40] | +[40] | PSA-independent NCAM function |
| LTP in CA3-CA1 synapse | –[34,39] | –[39] | –$,[44] | –#,[43] | +[42] | ST8Sia IV-dependent PSA-NCAM function |
| LTP in DG-CA3 synapse | +[42] | –[41] | +[44] | +[43] | +[42] | PSA-independent NCAM function |
| LTP in EC-DG synapse | n.d. | –[40] | n.d. | +[40] | +[40] | PSA-independent NCAM function |
| LTD in CA3-CA1 synapse | –[39] | n.d. | –$,[44] | –#,[43] | n.d. | ST8Sia IV-dependent PSA-NCAM function |

In 1996, Muller *et al.* indicated that the treatment of hippocampal slices with Endo-N resulted in the disappearance of LTP or LTD in the CA3-CA1 synapse (39). Then, several reports were published about analyses of PSA-NCAM in mice deficient in ST8Sia II, ST8Sia IV, and NCAM (Table I). In Table 1, STP shows an initial response following high frequency stimulation and LTP shows a long-lasting response for more than several minutes following stimulation. NCAM is involved in most of the synaptic plasticity of the three pathways of the hippocampus in Table 1, except for no response of STP in the DG-CA3 synapse (39–42).

First, LTP in the perforant pathway requires NCAM but not PSA (40). The expression of PSA-NCAM in one-third of postsynaptic density in the perforant pathway (35) has led to postulation of the involvement of PSA-NCAM in LTP and we expect progress in further investigations. Second, while PSA expressed depending on ST8Sia II is necessary for lamination of the mossy fiber, the STP and LTP in mossy fibers is PSA-independent (41,42), which might result from no expression of PSA in DG-CA3 synapses. Finally, LTP and LTD in the Schaffer collateral require PSA-NCAM (39, 42-45), which is not incongruous with the expression patterns of PSA-NCAM in pre- and post-synaptic membranes of CA3-CA1 synapses. Additionally, conditional ablation of NCAM by cre-recombinase under the control of the CAM kinase II promoter resulted in inhibition of LTP and LTD in the CA3-CA1 synapse (44). The ablation resulted from the recombinase activity in neurons involved in NMDA-dependent LTP, suggesting a correlation between PSA and NMDAR in the CA3-CA1 synapse. NMDAR consists of NR1 and NR2 subunits which are expressed in the pyramidal cells of the CA1 subfield. Recently, it has been reported that PSA-NCAM affected the NR2B subunit, that is, soluble PSA and PSA-NCAM inhibited single NMDAR channel activity stimulated by glutamate (46). The inhibition by PSA and PSA-NCAM was fully occluded by the NR2B-specific antagonist,

性の関連性を解説する。

1996年にMullerらは(39)、海馬スライスにEndo-N処理を行い、CA3-CA1シナプスにおけるLTPとLTDの消失を示した。このMullerらの報告の後、Endo-N処理に加えて、NCAM, ST8Sia II, ST8Sia IVのノックアウトマウス海馬における解析が行われてきた（表1)。表1におけるSTPとは、高頻度刺激後の初速時の反応を示し、LTPはその後数十分間にわたる長期増強を示している。NCAMは、苔状繊維におけるDG-CA3シナプスのSTPに関与しないことを除けば、海馬における3神経連絡のほとんどすべてのシナプス可塑性に関与している(39–42)。

貫通繊維路に関するLTPについては、NCAMは必須であるがPSAの影響を全く受けない。EC-DGシナプスの1/3がPSA-NCAMであることから(35)、PSAのシナプス可塑性への何らかの関与が示唆され、LTDを含めた今後の解析が待たれる(40)。次に苔状繊維の束化にはPSAの発現が関与し、特にST8Sia IIの発現が必須である(41,42)。その一方で、苔状繊維のLTPについては、PSAの影響を受けない。これは、DG-CA3シナプスにPSAの発現がないことから、シナプス可塑性には直接影響しないのかもしれない。さらにNCAMが、DG-CA3シナプスのSTPに作用しないことも、シナプスに発現していないことに関連するのかもしれない。最後に、シャファー側枝におけるシナプス可塑性は、PSA-NCAMのLTPやLTDへの影響をもっともよく説明している(39,42–45)。LTP及びLTD共に、PSA-NCAMの影響を強く受ける。これは、CA3-CA1シナプスの前シナプス膜及び後シナプス膜共にPSA-NCAMが分布していることからもシナプス可塑性への関与を裏付けることができる。また、NMDAR-dependent LTPの維持に重要であると考えられているCaM kinase IIのプロモーター支配下のCre遺伝子を用いた、コンディショナルNCAM欠失マウス海馬においても、CA3-CA1シナプスにおけるLTPとLTDが阻害された。こうした阻害は、NMDAR-dependent LTPに関与するニューロンにのみNCAMを欠失させた結果であることから、CA3-CA1シナプスにおけるNCAMとNMDARとの関連性を示唆することになる（44)。NMDARは、NR1とNR2サブユニットからなり、CA1錐体細胞には、NR2AとNR2Bの存在が知られているが、最近の知見から、PSA-NCAM